Ultrashort pulse propagation and Supercontinuum Generation in Silicon-on-Insultor Optical Nanowaveguides

Eric Rodrigue NUMKAM FOKOUA

Promotor(s)/Supervisor(s): Prof.Dr.Ir. Roel Baets, Dr.Ir. Wim Bogaerts
Assisting supervisor(s): Ir. Bart Kuyken

Master dissertation submitted in order to obtain the academic degree of

Erasmus Mundus Master of Science in Photonics

Academic year 2009-2010

UNIVERSITEIT GENT
Vrije Universiteit Brussel
KTH VETENSKAP OCH KONST ROYAL INSTITUTE OF TECHNOLOGY
HERIOT WATT UNIVERSITY
University of St Andrews

Ultrashort Pulse Propagation and Supercontinuum Generation in Silicon-On-Insulator optical nanowaveguides

Eric Rodrigue Numkam Fokoua

Promotoren: prof. dr. ir. Roel Baets, dr. ir. Wim Bogaerts
Begeleider: ir. Bart Kuyken

Masterproef ingediend tot het behalen van de academische graad van
Erasmus Mundus Master of Science in Photonics

Master dissertation submitted in order to obtain the academic degree of
Erasmus Mundus Master of Science in Photonics

Vakgroep Informatietechnologie
Voorzitter: prof. dr. ir. Daniël De Zutter
Faculteit Ingenieurswetenschappen
Academiejaar 2009-2010

UNIVERSITEIT GENT

Acknowledgments

Well, the past two years have been an incredible journey, the likes of which I never imagined myself undertaking. I have discovered and quite literally fell in love with Photonics. My personal growth, especially from an academic point of view, has been tremendous. For that I want to thank Professor Roel Baets for the incredible work he does, organizing and coordinating the Erasmus Mundus Master in Photonics programme. Special thanks go to him again for his meticulous supervision throughout this work, despite his busy schedule. For the always instructive discussions, for the trust placed in me in allowing me to work on this subject and for the willingness and enthusiasm in providing me the required equipment with which to work.

In my time in Scotland, Dr. Bruce Sinclair has been of tremendous help and his unique dedication and great attention to details have made the time in St Andrews very enjoyable. Professor Krauss has had a great contribution to my academic growth, and the work in St Andrews last summer provided a great opportunity to warm up for this thesis project.

Thanks to my supervisor Bart for his endless efforts and dedication, especially when things didn't work out. Thanks for the insightful discussions, and all the attention he gave throughout the work. I might have not been a fantastic thesis student, sometimes delaying tasks I should have completed on the get go, but he's always been patient enough. I want to thank Wim for his tips and insights, and obviously for the samples I worked on. I should also acknowledge Koen Huybrects for his thorough lab induction, teaching me how to use every piece of equipment in the lab in the first semester.

Stéphane Coen and stéphane Clemmen were kind enough to provide me with their MATLAB implementation of the propagation equation and a chapter of the then unpublished book on continuum generation, which contributed a lot to my understanding of the project.

Special thanks go to my fellow classmates, who have made the experience more fun and created a fantastic atmosphere in our office. Thanks to Stijntje, Sammeke, Arno, Jef,

Steven, Oliver, Thomas and Mohammed. Aimi has been a fantastic housemate and a great companion. The late-night chats, lunchtime discussions with Said, whether about Photonics or not, always provided me with great insight and have made the experience quite enjoyable. Thanks you folks for everything.

I want to thank my family, the support of whom cannot be overlooked. Thanks to my mother who despite battling sickness have provided me with all her love and support. Thanks to those taking care of her in place of me, making it possible for me to forget the worries and focus on my work here.

Finally, special thanks go to Jing, for all her unwavering love and support. It wouldn't all make much sense without her.

Thank you all,

Eric NUMKAM, June 2010

Toelating tot bruikleen

"De auteur geeft de toelating deze scriptie voor consultatie beschikbaar te stellen en delen van de scriptie te kopiëren voor persoonlijk gebruik.
Elk ander gebruik valt onder de beperkingen van het auteursrecht, in het bijzonder met betrekking tot de verplichting de bron uitdrukkelijk te vermelden bij het aanhalen van resultaten uit deze scriptie."

Permission to loan

The author gives his permission to make this work available for consultation and to copy part of the work for personal use. Any other use is bound to the restriction of copyright legislation, in particular regarding the obligation to specify the source when using results of this work.

Eric NUMKAM,
June 2010

Abstract

Continuum generation is a device functionality whereby an ultrashort pulse with high enough peak power is propagated in a nonlinear medium and undergoes significant spectral broadening to yield at the output a very broadband light signal. While such a light source has found application in may areas of scientific inquiry, it has been mainly achieved in silica fibers, which require extremely high peak powers and large lengths of fibre. In this work, we investigate how such a source can be implemented in a silicon nanowire. With its high cubic nonlinearity, and our ability to pattern it into planar waveguides with very small cross-sections and with control over their dispersion, continuum generation in silicon waveguides would require significantly lower peak powers and be achieved over just a few millimeters of propagation. We present here a theoretical model to describe nonlinear pulse propagation in silicon nanowaveguides as well as results from our experimental investigation of nonlinear effects in such structures.

Ultrashort pulse propagation and Supercontinuun generation in Silicon-on-Insulator optical Nanowaveguides

Eric R. Numkam Fokoua

Supervisor(s): Ir.Bart Kuyken, Prof.Dr.Ir. Roel Baets, Dr. Ir. Wim Bogaerts

Abstract— **In this work, we carry out both experimental and theoretical investigations of nonlinear light-natter interaction in silicon-on-insulator nanowire waveguides. We show how by engineering the dispersive properties of these waveguides, advantage can be taken of the high cubic nonlinearity $\chi^{(3)}$ of silicon in a way that both linear and nonlinear processes would affect a short pump pulse, leading to effects such as self-phase modulation, soliton formation, and continuum generation.**

Keywords— **Dispersion engineering, continuum generation, Kerr effect, two-photon absorption, free carrier dispersion**

I. Introduction

THE past few decades have seen silicon emerge as a material that can be used to guide and control light in the near infrared. The prospects of using silicon nanowires as optical interconnects on photonic integrated circuits have boosted much research into silicon photonics. As an optical material, silicon has unique properties that make it a viable candidate for nanoscale nonlinear optics. The high refractive index contrast in silicon-on-insulator(SOI) waveguides provide very tight light confinement. This tight confinement opens doors to devices with very small footprints and active control of linear dispersive properties. It offers the additional advantage of creating very high optical field densities, which combined with silicon's large third-order susceptibility in the near infrared, have led to the demonstration of nonlinear optical effects such as self-phase modulation, two-photon absorption, four-wave mixing and stimulated Raman scattering. With silicon's third-order susceptibility more than two orders of magnitude larger than that of typical fibres, these processes have been achieved at very modest power levels, over millimeter-long propagation distances.

Broadband light from continuum generation have found applications in precision metrology, coherence tomography and many other areas. Such light sources exploit are mostly based on microstructured fibers and require long propagation distances and very high peak powers. In the present work, we investigate how the interplay between linear and nonlinear effects of silicon waveguides can lead to continuum generation on chip-scale devices.

II. Dispersion Engineering in SOI waveguides.

Control over the dispersive properties of guiding devices is of utmost importance, as they govern the temporal profile of short pulses that propagate therein. In most of its transparent region and near 1.55 μm, bulk silicon has a large and normal group velocity dispersion. In a waveguide configuration however, mode confinement provide and additional component to the dispersion, which is highly dependent on the waveguide geometry. Applications such as continuum generation require careful choice of waveguide dimensions and accurate knowledge of the dispersion over a broad wavelength range. This information is obtained by using a full vectorial modesolver calculate the effective index for the optical mode of interest, which for us is the fundamental TE mode. In these calculations,material dispersion is included via the Sellmeier equation :

$$n^2(\lambda) = \varepsilon + \frac{A}{\lambda^2} + \frac{B\lambda_1^2}{\lambda^2 - \lambda_1^2} \tag{1}$$

where $\varepsilon = 11.6858$, $\lambda_1 = 1.1071\mu m$, $A = 0.939816\mu m^2$ and $B = 8.10461 \times 10^{-3}$ are specific material constants for silicon, and λ is in μm. Figure 1 shows plots of the group velocity dispersion coefficient, β_2 as a function of wavelength for various waveguide dimensions, along with that of bulk silicon. Clearly, choosing the proper waveguide dimensions is key to determine its dispersive properties. This freedom to tailor the dispersion at will is extremely valuable in implementing nonlinear optical devices for light conversion.

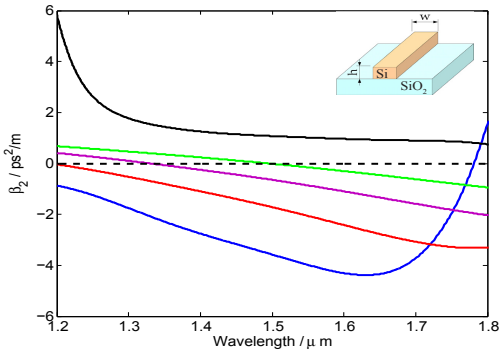

Fig. 1. GVD parameter for the fundamental TE mode as a function of wavelength. All the waveguides have the same height of $220nm$. The blue, red, purple and green curves correspond to $w = 450, 550, 650,$ and $750nm$ respectively. The black curve is the dispersion for bulk silicon.

III. Ultrashort pulse propagation in SOI waveguides

In SOI wire waveguides, a propagating short pulse high enough peak power creates an intensity dependent refractive index and generate free carriers through two-photon absorption (TPA). The generated carriers in turn affect further propagation by absorbing some of the photons (free carrier absorption ,FCA

) and by creating a small shift in the refractive index(free carrier dispersion, FCD). The pulse evolution in the waveguide is then governed by a nonlinear Schrödinger equation similar to the one used in fibres, but modified to account both for the high refractive index contrast, and all the effects absent in fibres. It is given as follows:

$$\frac{\partial a}{\partial z} = -\frac{\alpha}{2}a + i\sum_{m=2}^{m=\infty}\frac{i^m\beta_m}{m!}\frac{\partial^m a}{\partial T^m} + i\beta^f(\omega_0,\overline{N})a \qquad (2)$$
$$+ \; i\gamma_{eff}\left(1+i\tau_s\frac{\partial}{\partial T}\right)a(z,T)\int_{-\infty}^{\infty}d\tau R(T-\tau)\,|a(z,\tau)|^2$$

where $a(z,T)$ is the normalized pulse envelope. α represents the linear losses, mainly sidewall scattering and the infinite sum describes the dispersive properties. β_m are the m^{th} derivative of the propagation constant taken at the reference wavelength. The effective nonlinear parameter, $\gamma_{eff} = \frac{\omega n_2}{ca_{eff}} + i\frac{\beta_{TPA}}{2a_{eff}}$ embodies the nonlinear response of the waveguide. In its expression, $n_2 = 6\times10^{-18}m^2/W$ is the kerr coefficient, $\beta_{TPA} = 5\times10^{-12}m/W$ the two-photon absorption, and a_{eff} the effective modal area. The parameter τ_s called the shock is responsible for optical shock formation and self-steepening, while the function $R(\tau)$ is the time domain Raman response of silicon. The term with β^f governs free carrier effects, and is proportional to the average over the mode cross-section of the TPA-generated free carriers density $\overline{N}$, the time dependence of which is given by:

$$\frac{\partial\overline{N}}{\partial t} = \frac{\beta_{TPA}}{2\hbar\,\omega a_{eff}^2}\,|\mathbf{a}(z,t)|^4 - \frac{\overline{N}}{\tau_c} \qquad (3)$$

Coupled equations (2) and (3) completely describe the dynamics of pulse propagation in Si wire waveguides. To model pulse propagation, we solve them numerically by implementing a form of the split-step fourier algorithm. The frequency dependence of the nonlinear parameter γ_{eff} is not explicitly included in our modeling. Figure 2 shows an example of such simulations.We propagate a pulse with $T_0 = 100fs$ and $P_0 = 3.7W$ in a centimeter-long Si wire with $750\times220nm^2$ cross-section. These pulse and waveguide parameters are chosen such that, the soliton number $N^2 = \gamma_{eff}P_0T_0^2/\,|\beta_2| \sim 3$. The launched pulse thus corresponds to a third-order soliton, given that $\beta_2 < 0$. As can be seen from the figure, after propagation over just a centimeter, the original pulse breaks down into its constituents solitons, with the generation a dispersive wave generation at the back of the pulse. The result is is a broadband continuum that extends over $400nm$.

IV. Experimental investigations of pulse propagation in SOI waveguides

With their very high nonlinear parameter and their small cross-sections, SOI wires are driven into a strong nonlinear regime by very modest input powers. On the other hand,nonlinear processes are inherently limited in that, increasing pump powers induce greater nonlinear losses from TPA in the first steps of propagation. This has been referred to as optical limiting. For the experimental part of our work, we couple

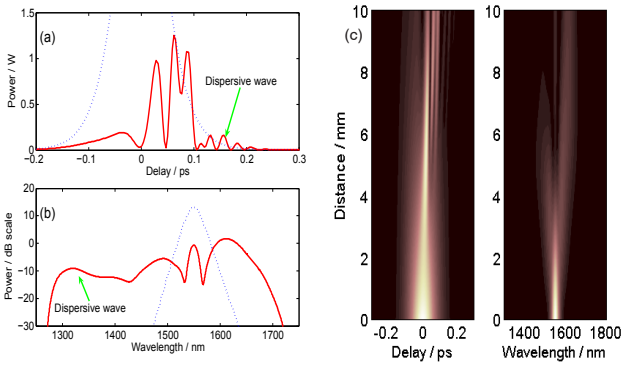

Fig. 2. Soliton fission and continuum generation in a centimeter long, $750\times220nm^2$ Si wire. (a) Time domain input(dash blue) and output (red) pulse profile. (b) Spectrum at input(dash-blue) and output (red). (c) Density plot of pulse evolution along the waveguide length.

picosecond and femtosecond pulses centered at $1.55\mu m$ in the designed waveguides. The waveguide output is connected to a powermeter and a spectrum analyzer. Fig. 3 shows our experimental demonstration of SPM with ps pulses in SOI wires, along with spectra resulting from femtosecond pulse propagation. Simulations agree well with experiment in the former case, but not so well in the latter, a fact we attribute to our short pulse source not being optimized for the experiments.

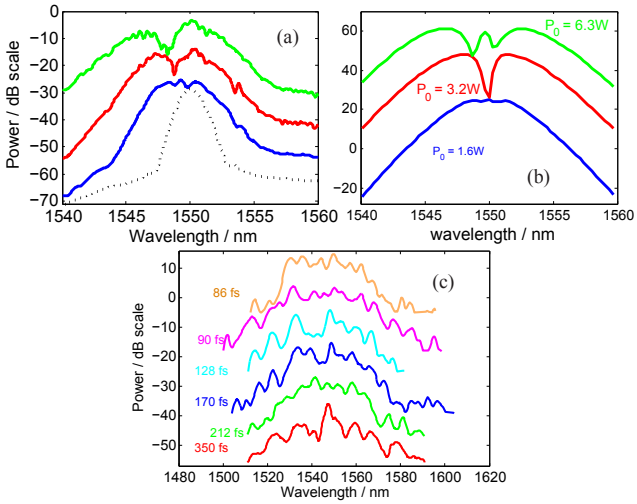

Fig. 3. Experimental pulse propagation in Silicon wires. (a) SPM with $1.8ps$ pulses and shown peak powers propagated in $1cm-$long, $650\times220nm^2$. (b) corresponding simulations. (c) $20dB$ bandwith of recorded spectra at the output of $1cm-$long, $750\times220nm^2$ pumping with femtosecond pulses.

V. Conclusion

We have carried out both theoretical and experimental study of short pulse propagation in SOI wire waveguides. While some of the effects observed are in good agreement with numerical modeling, broadband light generation from femtosecond pump pulses as predicted from theory has yet to be demonstrated experimentally

Contents

Title Page i

Acknowledgments iv

Toelating tot bruikleen vi

Abstract vii

Extended abstract x

Table of Contents xi

List of Figures xii

1 Introduction 1
1.1 Overview of the thesis . . . 2

2 Light Matter Interaction in Silicon Photonic wires 4
2.1 Linear properties of silicon waveguides . . . 4
2.1.1 Silicon photonic wires and means to interrogate them . . . 4
2.1.2 Dispersion Engineering in Silicon Photonic Wires . . . 6
2.1.3 Linear propagation losses in Silicon waveguides . . . 11
2.2 Nonlinear processes in Silicon Photonic Wires . . . 12
2.2.1 Nonlinear polarization and Third-order susceptibility of silicon . . . 12
2.2.2 The Kerr effect and Two-photon absorption . . . 13
2.2.3 Free Carrier effects . . . 15
2.2.4 The Raman Response . . . 17
2.3 Summary . . . 17

3 Theory of ultrashort pulse propagation in Silicon Photonic Wires. 19
3.1 Frequency domain propagation equation . . . 19
3.2 Time domain Formalism . . . 25

3.3 Numerical solution to the Propagation equation . . . 27
3.4 Model Validation . . . 30
3.5 Summary . . . 33

4 Dynamics of continuum generation in Si photonic wires 34
4.1 Relative Importance of nonlinear and dispersive effects in Si photonic wires. . . . 34
4.2 Self-phase modulation in SPWs . . . 35
4.3 Soliton dynamics in SPW . . . 38
4.4 Four-wave mixing and Modulation Instability . . . 43
4.5 Limiting nature of continuum generation in Si photonic wires . . . 44
4.6 Summary . . . 46

5 Experimental investigation of nonlinear processes in Si photonic Wires 47
5.1 Picosecond pulse propagation in Si photonic wires . . . 47
5.1.1 Experimental setup . . . 47
5.1.2 Self-phase modulation using picosecond pulses . . . 49
5.1.3 Further broadening with picosecond pulses . . . 51
5.1.4 Optical Limiting with picosecond pulses . . . 54
5.2 Femtosecond pulse propagation in Si photonic wires . . . 55
5.2.1 Source characterization . . . 55
5.2.2 Results with non-attenuated pulses . . . 56
5.2.3 Measurements with attenuated pulses . . . 60
5.3 Summary . . . 63

6 Conclusion and Outlook 64

Conclusion and Outlook 64

A Dispersion coefficients for the wire waveguides used in this work 66

Bibliography 67

List of Figures

2.1 Silicon Photonic Wire . . . 5
2.2 Coupling Schemes for the SPWs . . . 7
2.3 TE and TM mode field distribution . . . 8
2.4 Effective index data for several waveguide widths . . . 9
2.5 GVD coefficient for 350 to 500 nm wide waveguides . . . 10
2.6 GVD coefficient for 550 to 850 nm wide waveguides . . . 11
2.7 Measured data for Kerr and TPA coefficients . . . 16
2.8 Light matter interaction in Silicon . . . 18

3.1 Modeling of Soliton fission and SCG in silicon waveguides . . . 31
3.2 Density plot of pulse propagation in$360 \times 220nm^2$ SPW . . . 32

4.1 Self-phase Modulation of a ps pulse in a $450 \times 220nm^2$ SPW . . . 36
4.2 Self-phase Modulation of a $200fs$ in a $450 \times 220nm^2$ SPW . . . 37
4.3 Self-phase Modulation in normal and anomalous GVD . . . 39
4.4 Soliton fission in a Si Photonic wire . . . 41
4.5 Dispersive wave generation in a Si Photonic wire . . . 42
4.6 Four-wave mixing . . . 43
4.7 Demonstration of the Limiting nature of continuum generation in SPWs . 45

5.1 Experimental Setup . . . 48
5.2 Experimental SPM in $450 \times 220nm^2$, $5mm$ long wire . . . 50
5.3 Experimental SPM in $650 \times 220nm^2$, $10mm$ long wire . . . 51
5.4 Picosecond pulse broadening in $450 \times 220nm^2$, $10mm$ long wire . . . 52
5.5 Picosecond pulse propagation in $450 \times 220nm^2$, $1cm$ long wire comparison with model . . . 53
5.6 Optical Limiting in Si photonic wires with picosecond pulses . . . 54
5.7 Setup for femtosecond pulse experiments . . . 56
5.8 Femtosecond Source spectra after propagation in various lengths of fiber$30cm$ of fiber . . . 57
5.9 Recorded spectra with a $350 \times 220nm^2$, $1cm$ long waveguide . . . 58

5.10 Recorded with a $350 \times 220nm^2$, $1cm$ long waveguide 59
5.11 Recorded spectra with a $750 \times 220nm^2$, $1cm$ long waveguide 60
5.12 Femtosecond source spectra with a $15dB$ attenuator at the output of the source 61
5.13 Pulse propagation in 550 and $750 \times 220nm^2$ wires. 62
5.14 Modeling spectra for propagation in 550 and $750 \times 220nm^2$ wires. 63

Chapter 1

Introduction

With the invention of the laser by Theodore Maiman in 1960 and the demonstration of second harmonic generation the following year was born the field of Nonlinear Optics. Since, it has emerged as a great success of modern optics. The observation of nonlinear phenomena require high optical intensities, nearly monochromatic sources with good control over their coherence properties, and the laser just fits those criteria. Developments both in the nonlinear materials side as well as the laser source have allowed for an unprecedented control over the way light interacts with matter and have led to hundreds of practical applications, among which Raman spectroscopy, wavelength converters and supercontinuum generation.

Parallel to these major advances, the technology that we use to send information around the world in forms of light pulses transmitted in silica optical fibres matured. Low-order nonlinear optical effects as we shall see, are created because the dependence of the polarization induced in a propagation medium by an electric field ceases to be linear when intensities are high. When such condition are met, the medium can be characterized by its nonlinear susceptibility. Though very small, the third order susceptibility $\chi^{(3)}$ of silica fibres is not negligible, and is not only responsible for the effects such as self-phase modulation and four wave mixing observed in fibres, but for the whole field of nonlinear fibre optics as well. Making use of these nonlinear effects in real devices requires either the use of very high power sources, very long lengths of fibre,or that we shrink the core size of fibre core to very small dimensions.

These inconveniences, along with the need to miniaturize and integrate optical components on chips, have in turn given birth to what has been called nanoscale nonlinear optics. As the name indicates, the focus has been on the study of in-plane nonlinearities of dielectric materials patterned into nanometer size guiding structures. With its attrac-

tive electronic and optical properties, as well as the backing of the CMOS manufacturing technology, silicon seems to be one such material. In fact, the last few decades have seen tremendous progress in silicon photonics. Simple guiding structures, active optical devices such as modulators and raman lasers have been successfully implemented in silicon. Furthermore, the prospects of integration with silicon-based CMOS electronics now make the idea of microprocessors with optical interconnects not so far-fetched.

The present work aims to investigate the nonlinear optical processes that occur when very short pulses of light in the ps or fs regime propagate in nanometer-scale silicon-on-insulator waveguides. With their cross-sections smaller than the wavelength used here, $1.55\mu m$, the dispersive properties of these structures have a strong waveguide dispersion component, opening the way to dispersion engineering. Furthermore, the strong confinement due to the refractive index contrast also results in very high effective nonlinear susceptibility $\chi^{(3)}_{eff}$. The main goal has been to study how to control dispersive and nonlinear properties so as to experimentally implement the device functionality whereby short pulses would undergo severe spectral broadening, known as supercontinuum generation.

1.1 Overview of the thesis

The thesis is structured as follows. In Chapter 2, we introduce the silicon photonic wires, discuss their dispersive properties and show how dispersion can be engineered through properly selecting waveguide dimensions. The fully vectorial modesolver FimmWave is used to calculate the effective index across the wavelength range of interest, and dispersion information is extracted. We also introduce here the major nonlinear effects stemming from the cubic susceptibility of silicon. We define the nonlinear polarization and discuss its effects on pulse propagation.

In Chapter 3, we present a theoretical formulation of short pulse propagation in silicon waveguides. A propagation equation is derived and a numerical model to solve it is built.

Chapter 4 goes on to discuss the major processes that in Si wires lead to spectral broadening and continuum generation. We use our numerical model to demonstrate the possibility of self-phase modulation, soliton formation and continuum generation. We also discuss the optical limiting phenomenon that is characteristic of nonlinear media when strong nonlinear absorption is present.

Finally, Chapter 5 covers our experimental work on nonlinear effects in SPWs, with

comparison to simulation made whenever appropriate. A short conclusion then follows.

Chapter 2

Light Matter Interaction in Silicon Photonic wires

In this chapter, we discuss the fundamentals of light-matter interaction and the nonlinear processes that occur as an ultrashort pulse of light propagates in a silicon waveguide. Before we get there however, we introduce the linear optical properties of such wires, focussing on how their design affect their guiding properties such as modal field distribution and effective refractive index. What is of interest in so doing as we shall point out is the frequency dispersion of the propagation constant.The nonlinear processes that contribute to the spectral broadening we wish to achieve often depend on phase-matching conditions, and efficient continuum generation relies on our ability to engineer dispersion to all orders.

2.1 Linear properties of silicon waveguides

2.1.1 Silicon photonic wires and means to interrogate them

By Silicon Photonic Wires (SPWs) or Silicon waveguides, we refer to the ridge waveguide structure that can be seen in Figure 2.1 below. Such structures were pioneered by Soref and Lorenzo, who first demonstrated the use of silicon as a material for guiding light in the telecom wavelengths in 1985. The wire made of silicon is patterned on a $1\mu m$ thick layer of silica (SiO_2), which itself reposes on a thicker silicon substrate.

The wire waveguides used in this work are from the CMOS production line at IMEC-Leuven, and all have a height $h = 220nm$ for the silicon core layer. Therefore, the only parameters that remains available to modify and engineer dispersion is the waveguide

width w, which will typically have values between 350 and 850nm.

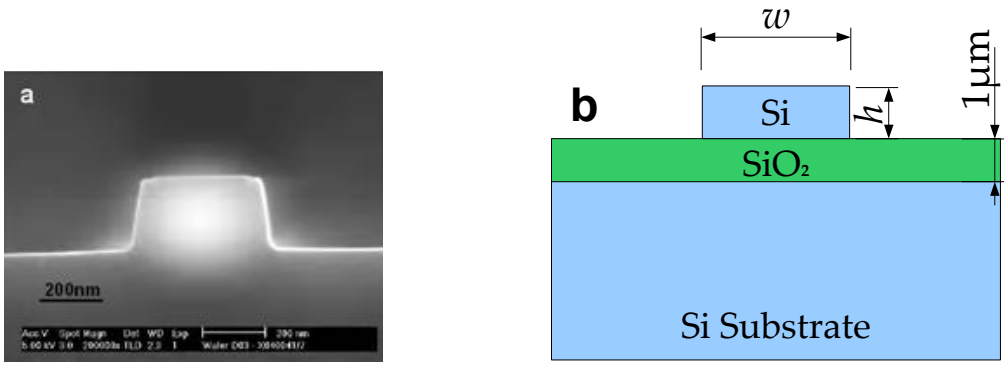

(a) (b)

Figure 2.1: (a) SEM image of cross section. (b) graphical illustration of structure

When propagating through such a structure, light is trapped in the silicon wire through total internal reflection because of the high refractive index contrast between the silicon core ($n = 3.476$), the underlying silica cladding layer ($n = 1.444$) and the top cladding layer which throughout this work is air, but could be any other low-index material such as polymers or chalcogenide glasses. The field distribution in the plane of the cross-section, which is a solution of Maxwell's equation, will be called an optical *mode*. Our waveguides normally support transverse electric (TE) modes and transverse magnetic (TM) modes. The TE modes have their electric $\overrightarrow{\mathbf{E}}$-field oscillating in the plane, while the TM mode have their magnetic $\overrightarrow{\mathbf{H}}$-field oscillating in-plane.

To characterize such waveguides, we need to efficiently couple light both in and out. To do this, two configurations are used and are shown in Figure 2.2 below. Our waveguides have incorporated on them grating coupler structures which allow to couple light in and out vertically from slightly tilted fibers (8 to 10°). Those are one-dimensional gratings etched in a 10-12μm broad waveguides, which are then linearly tapered down to the width of our waveguide. One problem that arises when grating couplers are used at both ends, is that their spectral bandwidth is limited. And for applications such as continuum generation where we seek to generate very broadband light, it is problematic, as much of the light generated through non-linear processes might not make it to the detector. That is why some of our samples have been cleaved to get rid of the out-

put grating coupler. Light at the output can then be collected, though less efficiently, through butt coupling with a fiber or a microscope objective as displayed in Figure. The gratings are designed to give optimum performance at a wavelength of $1550nm$, which is the used throughout the experiments in this work. The gratings are also optimized to couple more efficiently to the fundamental **TE** mode and the linear taper ensures that light propagating inside our waveguide will mostly be that mode, even when the width is such that it is possible to support other modes.

2.1.2 Dispersion Engineering in Silicon Photonic Wires

As we pointed out earlier, control of dispersion is crucial in order to implement the kind of device functionalities we're looking for, such as wavelength conversion or continuum generation. Dispersion dictates the temporal properties of ultrashort pulses as they propagate inside the waveguides, whether or not pulses form temporal solitons for example will depend on whether the group velocity dispersion is anomalous or not.

The very high index contrast in the SOI structure that we use throughout this work means that the electromagnetic field propagating in the core will experience very strong confinement. This has a number of advantages as mentioned in the introduction. First of all, it ensures that the waveguide geometry is actually governing the dispersive properties of the waveguide, and second as we shall see, it lowers the power requirements in order to observe strong nonlinear effects.

Dispersion engineering has been demonstrated in microstructured fibers, and multimode fibers for example. The same has been done in SPWs, first by Chen et al [1] who showed such wires could be designed to have zero group velocity dispersion (ZGVD) around telecommunication wavelengths.

To show how dispersion changes as a function of the only parameter available to us to tune, namely the waveguide width w, we use the fully vectorial 3D modesolver software FimmWave to compute the effective refractive index n_{eff}, again for the fundamental TE mode which will be the one actually propagating in our waveguide. An example of the field distribution as computed by Fimmwave is shown in the Figure below. We then extract the propagation constant given by:

$$\beta(\omega) = \frac{n_{eff}(\omega)\omega}{c}. \tag{2.1}$$

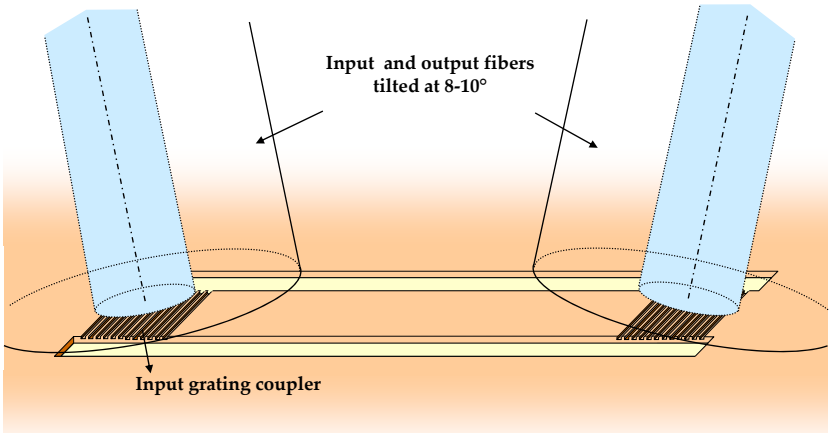

(a)

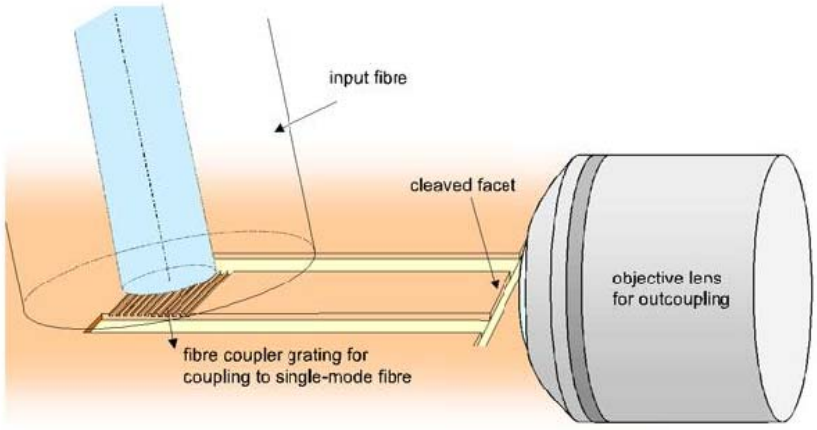

(b)

Figure 2.2: (a) Vertical fiber coupling in and out (b) vertical in coupling, horizontal out-coupling

Once we obtain the propagation constant $\beta(\omega)$, the group index $n_g = c/v_g = \beta_1 c$ with v_g being the mode's group velocity,the group velocity dispersion parameter β_2 and the third order dispertion coefficient β_3 will all be readily obtained. All order dispersion coefficients are simply given by:

$$\beta_n = \frac{d^n \beta(\omega)}{d\omega^n} \tag{2.2}$$

The commonly used dispersion parameter D is related to the GVD coefficient as : $D = -\frac{2\pi c \beta_2}{\lambda^2}$, where λ is the wavelength and D is given in $ps/nm \cdot km$.

Fimmwave calculations fully account for the material dispersion of both the silicon core layer and the silica cladding layer through their Sellmeier equation which take the form:

$$n^2(\lambda) = \varepsilon + \frac{A}{\lambda^2} + \frac{B\lambda_1^2}{\lambda^2 - \lambda_1^2} \tag{2.3}$$

for silicon, the constants appearing in this equation are : $\varepsilon = 11.6858$, $\lambda_1 = 1.1071 \mu m$,

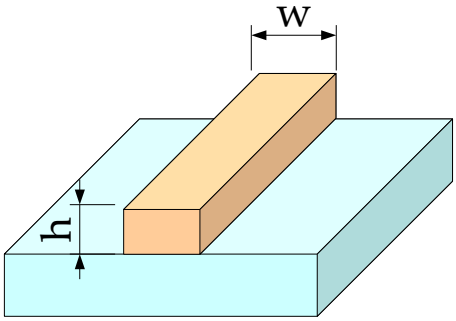

(a)

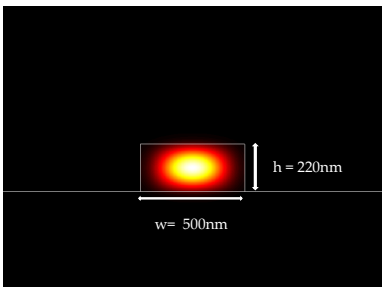

(b)

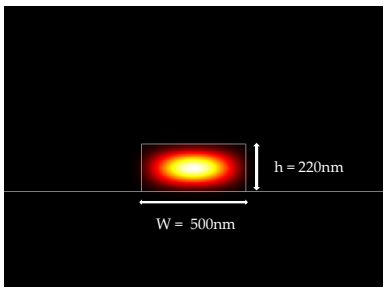

(c)

Figure 2.3: (a) Actual structure (b) TE mode intensity profile (c) TM mode intensity profile

$A = 0.939816\mu m^2$ and $B = 8.10461 \times 10^{-3}$. Figure 2.4 below shows the effective index for several waveguide widths as computed by FimmWave.

The effective index is calculated between $\lambda = 1.2$ and $\lambda = 2\mu m$, which is our range of interest, for the fundamental TE mode. It is defined by:

$$n_{eff}(\lambda) = \frac{\beta(\omega)}{k_0} \tag{2.4}$$

where $\beta(\omega)$ is the propagation constant obtained by solving Maxwell's equations with the appropriate boundary conditions, and $k_0 = 2\pi/\lambda$ is the free space propagation constant.

It can be seen on the plots of Figure 2.4 that, for shorter wavelengths, the confinement provided by waveguides of different size is almost the same, and thus the little difference in effective index. As wavelength increases, this ceases to be the case, thus n_{eff} does have a strong waveguide contribution. To proceed, we fit the refractive index data with a 9-degree polynomial and calculate its derivatives. Up to the second or-

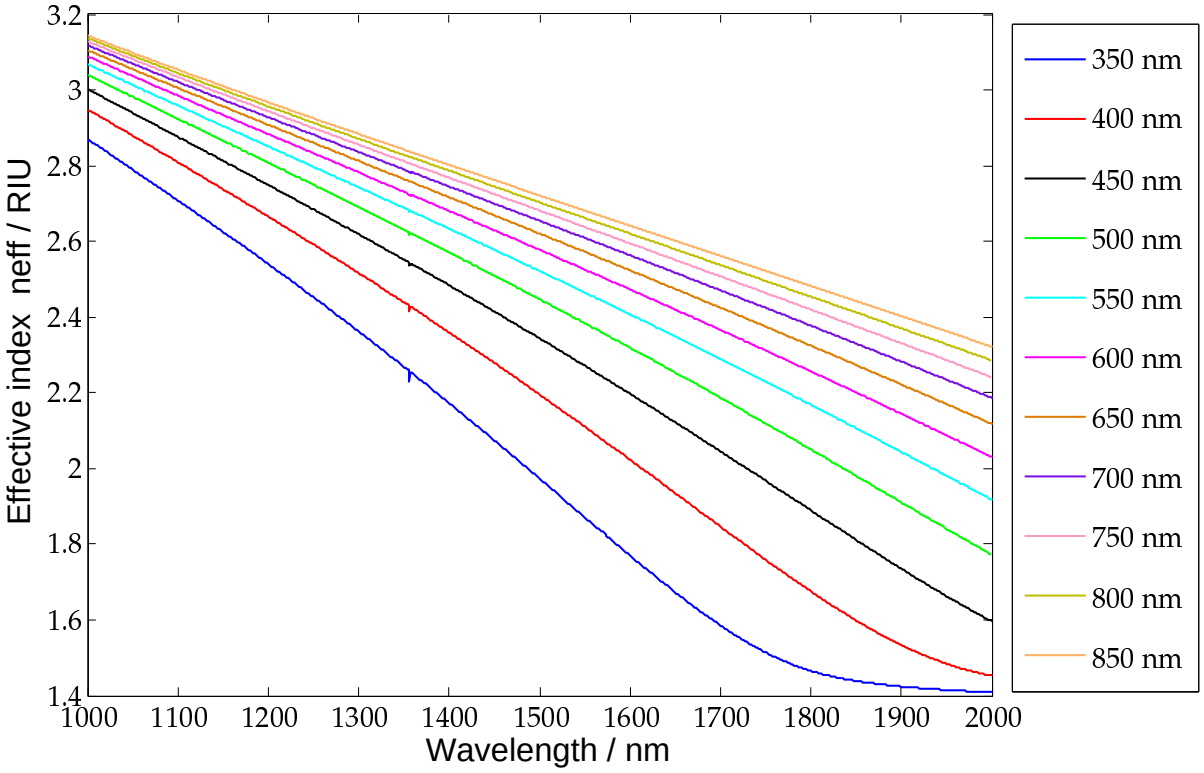

Figure 2.4: Fundamental TE mode Effective index for different SPWs

der, the dispersion coefficients obtained from this method can be considered accurate. However, as pointed out by Dadap et al [2], because of the accumulative errors due to successive derivation steps, coefficients beyond the second order are not accurate and must be determined experimentally. This is done for example by tracking solitonic features in experimental data.

For the waveguide dimensions used in this work, SPWs display two zero dispersion wavelengths (ZDW). Figures 2.5 and 2.6 below shows the group velocity dispersion coefficient, rather $-\beta_2$ as obtained from the n_{eff} data. For smaller waveguides, it is the second ZDW that is of interest, and it can be shown here that a waveguide slightly wider than $350nm$ will have its ZDW exactly at $1.55\mu m$, which is in agreement with the value $w = 360nm$ found by Osgood et al. For wider waveguide however, it is the first ZDW that is of interest. The two ZDWs can be clearly seen for the $w = 550nm$ waveguide.

It can be seen from the plots that both ZDWs shift to the red as a result of increasing waveguide width. We will not show here the plots of higher order dispersion coefficient, but their value at $1550nm$ which will be our pump wavelength, is tabulated and

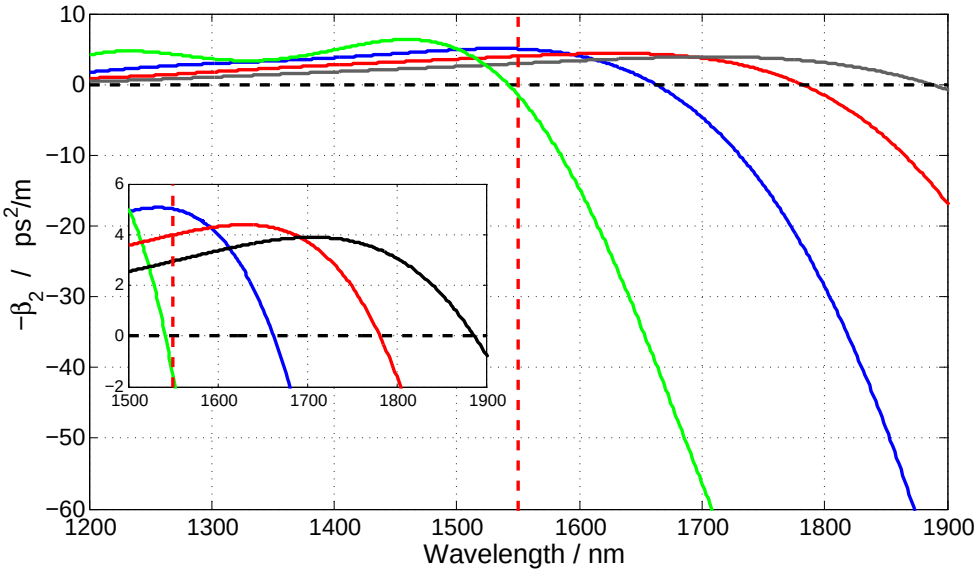

Figure 2.5: Group velocity dispersion coefficient $-\beta_2$ as function of wavelength for the fundamental TE mode. Green curve is for $w = 350nm$, the blue for $w = 400nm$, the red for $w = 450nm$ and the black curve for $w = 500nm$. The inset zooms on the area where $\beta_2 = 0ps^2/m$

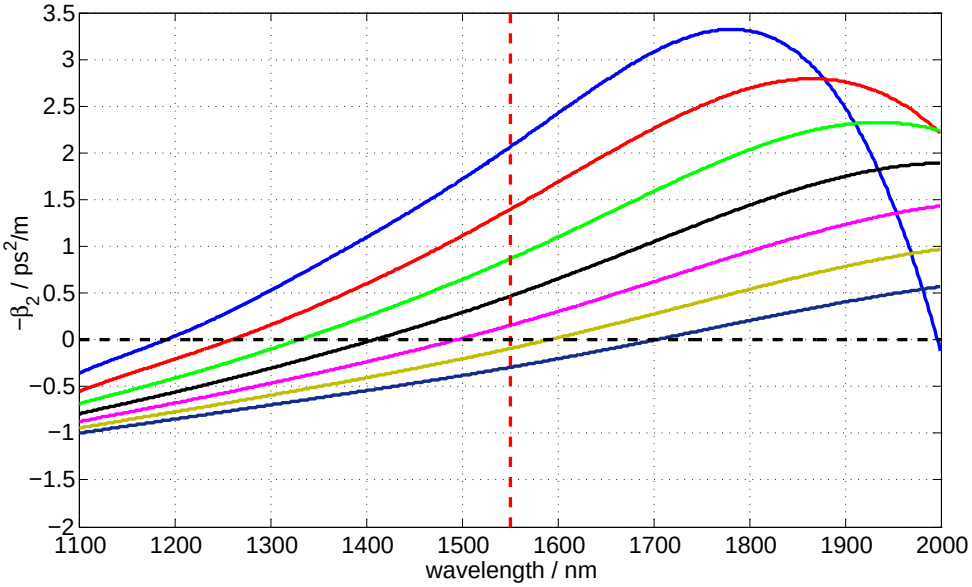

Figure 2.6: Group velocity dispersion coefficient $-\beta_2$ as function of wavelength for the fundamental TE mode. From left to right are the $w = 550nm$ to $w = 850nm$ in $50nm$ increments.

can be found in the appendix. We close this section by alluring to something we shall discuss at length, namely that experiments in microstructured fibers have revealed that most efficient continuum generation is achieved when the waveguide is pumped in the vicinity of its ZDW wavelength, but in the anomalous dispersion regime($\beta_2 < 0$). Most of our waveguides of Figure 2.6 do have $1550nm$ in the anomalous GVD regime, with the $w = 750nm$ having the closest ZDW to $1550nm$. SPWs however are different from fibers, and as a result, effective nonlinear susceptibilities are in fact lower for wider waveguides.

2.1.3 Linear propagation losses in Silicon waveguides

As light propagates in our waveguide, we can expect propagation losses to arise from a number of reasons.Bulk and surface state absorption are not expected to be significant in the wavelength range we use. Rayleigh scattering and substrate leakage are another source, though they will again be neglected. The dominant contribution to linear loss comes from scattering at sidewall roughnesses. The overall loss value as taken from ref [4] will be 3 to $3.5dB/cm$.

2.2 Nonlinear processes in Silicon Photonic Wires

We have pointed out earlier that low-order nonlinear effects occur in dielectric media when the intensity of the propagating field is so strong that the media polarization ceases to be linear with the field. In SPWs, because of the tight confinement due to the high index contrast and their very small cross-section, such high intensities can be easily achieved with modest power levels. In addition, the nonlinear response of silicon is orders of magnitude stronger than that of silica fibers for example. We will in this section introduce the main nonlinear effects that will affect pulse propagation, and mathematical formulation of pulse propagation will be given and discussed in a future chapter.

2.2.1 Nonlinear polarization and Third-order susceptibility of silicon

When the intensity of the propagating field is high enough, the induced polarization inside the SPW can be expressed as a power series of the electric field:

$$\mathbf{P}(t) = \mathbf{P}^{(0)}(t) + \mathbf{P}^{(1)}(t) + \mathbf{P}^{(2)}(t) + \mathbf{P}^{(3)}(t) + \cdots \tag{2.5}$$

or equivalently in the fequency domain:

$$\mathbf{P}(\omega) = \mathbf{P}^{(0)}(\omega) + \mathbf{P}^{(1)}(\omega) + \mathbf{P}^{(2)}(\omega) + \mathbf{P}^{(3)}(\omega) + \cdots \tag{2.6}$$

where $\mathbf{P}^{(0)}$ is independent of the field and $\mathbf{P}^{(n)}$ is proportional to $(\mathbf{E})^n$. Furthermore, time and frequency domain fields are related via a Fourier transform:

$$\mathbf{P}^{(n)}(\omega) = \mathfrak{F}\left(\mathbf{P}^{(n)}(t)\right) = \int_{-\infty}^{\infty} \mathbf{P}^{(n)}(t) \exp(-j\omega t) dt \tag{2.7}$$

$$\mathbf{P}^{(n)}(t) = \mathfrak{F}^{-1}\left(\mathbf{P}^{(n)}(\omega)\right) = \frac{1}{2\pi} \int_{-\infty}^{\infty} \mathbf{P}^{(n)}(\omega) \exp(j\omega t) d\omega \tag{2.8}$$

Under the conditions of time invariance and causality, the n-th order polarization is given by (reference):

$$\begin{aligned} \mathbf{P}^{(n)}(\omega, \mathbf{r}) &= \epsilon_0 \left(\frac{1}{2\pi}\right)^{n-1} \int_{-\infty}^{\infty} d\omega_1 \cdots \int_{-\infty}^{\infty} d\omega_n \cdot \chi^{(n)}(-\omega_\sigma; \omega_1, \cdots, \omega_n) \\ &\vdots \mathbf{E}(\mathbf{r}, \omega_1) \cdots \mathbf{E}(\mathbf{r}, \omega_n) \delta(\omega - \omega_\sigma) \end{aligned} \tag{2.9}$$

where $\chi^{(n)}$ is the n-th order susceptibility tensor. These tensors depend on the nature and crystalline structure of the dielectric medium. They vanish quicly as n increases,

and thus are rarely considered beyond the third order. Crystalline silicon has a centrosymmetric structure as it belongs to the $m3m$ class, and as such, its even order susceptibilities are identically zero. That leaves us with the lowest order-nonlinear susceptibility being the third-order one, and it is the source of the effects investigated in this work.

If we now consider a monochromatic wave of frequency ω propagating in our SPW, that is:

$$\mathbf{E}(\mathbf{r},t) = \frac{1}{2}E_\omega(\mathbf{r},t)\exp(j\omega t) + c.c \tag{2.10}$$

then the polarization response can have frequencies ω, $-\omega$ for the first order, and 3ω, -3ω as well as ω and $-\omega$ for the third order. Because of phase-matching requirements, the third-order harmonic generation process that leads to waves at 3ω is very inneficient and neglected. When such conditions as well as that of permutation symmetry are satisfied, the total response at frequency ω as obtained from equation (2.9) is :

$$\mathbf{P}(\mathbf{r},\omega) = \epsilon_0\chi^{(1)}\cdot\mathbf{E}(\mathbf{r},\omega) + \frac{3}{4}\epsilon_0\chi^{(3)}(-\omega;\omega,-\omega,\omega)\vdots\mathbf{E}(\mathbf{r},\omega)\mathbf{E}^*(\mathbf{r},\omega)\mathbf{E}(\mathbf{r},\omega) \tag{2.11}$$

$\chi^{(3)}$ is a third-order susceptibility tensor, the real part of which will lead to a nonlinear refractive index or the Kerr effect, and its imaginary part will cause nonlinear loss via two-photon absorption or TPA. The tensor normally has 81 elements, but for $m3m$ crystals like silicon however, only 21 elements of the tensor are nonzero, of which only 4 are independent, namely : $\chi^{(3)}_{1111}$, $\chi^{(3)}_{1122}$, $\chi^{(3)}_{1212}$and $\chi^{(3)}_{1221}$. Symmetry of the crystal also requires that $\chi^{(3)}_{1122} = \chi^{(3)}_{1221}$, and if we neglect frequency dispersion of the tensor as we will always do throughout this work, Kleinman symmetry is valid and $\chi^{(3)}_{1122} = \chi^{(3)}_{1212}$. Therefore only two elements will be truly independent. Different effects will contribute to the ultimate values of the susceptibility, with the most important being the bound electronic Kerr effect, and the Raman response.

2.2.2 The Kerr effect and Two-photon absorption

Let's consider for the moment that in equation (2.11) the nonlinear susceptibilities are scalars. Then we have:

$$\begin{aligned}\mathbf{P}(\mathbf{r},\omega) &= \epsilon_0\chi^{(1)}\cdot\mathbf{E}(\mathbf{r},\omega) + \frac{3}{4}\epsilon_0\chi^{(3)}(-\omega;\omega,-\omega,\omega)\cdot|\mathbf{E}(\mathbf{r},\omega)|^2\,\mathbf{E}(\mathbf{r},\omega)\\ &= \epsilon_0\left(\chi^{(1)} + \chi^{(3)}(-\omega;\omega,-\omega,\omega)\cdot|\mathbf{E}(\mathbf{r},\omega)|^2\right)\mathbf{E}(\mathbf{r},\omega)\end{aligned} \tag{2.12}$$

with the complex refractive index $n_c(\omega) = n - jK$ defined from the relation :

$$\mathbf{P}(\mathbf{r},\omega) = \epsilon_0\left(n_c^2(\omega) - 1\right)\mathbf{E}(\mathbf{r},\omega) \tag{2.13}$$

we therefore have, as $n \gg K$:

$$\begin{aligned} n &\approx \sqrt{1 + Re\chi^{(1)} + \frac{3}{4} Re\chi^{(3)}(-\omega;\omega,-\omega,\omega) \cdot |\mathbf{E}(\mathbf{r},\omega)|^2} \\ &\approx \sqrt{1 + Re\chi^{(1)}} + \frac{3}{8} \frac{Re\chi^{(3)}(-\omega;\omega,-\omega,\omega) \cdot |\mathbf{E}(\mathbf{r},\omega)|^2}{\sqrt{1 + Re\chi^{(1)}}} \\ &\equiv \sqrt{1 + Re\chi^{(1)}} + \frac{3}{4} \frac{Re\chi^{(3)}(-\omega;\omega,-\omega,\omega) \cdot I_\omega}{\epsilon_0 c n_0 \sqrt{1 + Re\chi^{(1)}}} \\ &\equiv n_0 + n_2 \cdot I_\omega \end{aligned} \tag{2.14}$$

where

$$n_0 \equiv \sqrt{1 + Re\chi^{(1)}} \tag{2.15}$$

and

$$n_2 \equiv \frac{3 Re\chi^{(3)}(-\omega;\omega,-\omega,\omega)}{4 n_0^2 \epsilon_0 c} \tag{2.16}$$

On the other hand, we do have:

$$\begin{aligned} K &\approx -\frac{Im\chi^{(1)}}{2n_0} - \frac{3 Im\chi^{(3)}(-\omega;\omega,-\omega,\omega)\,|\mathbf{E}_\omega|^2}{8 n_0} \\ &\equiv -\frac{Im\chi^{(1)}}{2n_0} - \frac{3 Im\chi^{(3)}(-\omega;\omega,-\omega,\omega) \cdot I_\omega}{4 n_0^2 \epsilon_0 c} \\ &\equiv K_0 + K_2 \cdot I_\omega \end{aligned} \tag{2.17}$$

where again

$$K_0 \equiv -\frac{Im\chi^{(1)}}{2n_0} \tag{2.18}$$

and

$$K_2 \equiv -\frac{3 Im\chi^{(3)}(-\omega;\omega,-\omega,\omega)}{4 n_0^2 \epsilon_0 c} \tag{2.19}$$

K_0 and K_2 relate to the linear and two photon absorption coefficients as $\alpha = 2\frac{\omega}{c} K_0$ and $\beta_{TPA} = 2\frac{\omega}{c} K_2$.

What we have just derived in equations (2.16) and (2.19) is remarkable. First of all, it means that a wave propagating inside our waveguide will induce an additional intensity-dependent component to the refractive index. This is the Kerr effect and is the origin of self-phase and cross-phase modulation when short pulses propagate in

the waveguide. Though the photon energy might not be high enough to put a valence band electron into the conduction band via a simple transition, two photons can be absorbed at the same time and result in such a transition as long as $\hbar\omega \geqslant \frac{E_g}{2}$. This is the two-photon absorption process. It constitutes in itself a source of loss for a pulse propagating inside the waveguide, but free carriers it generates will also affect pulse propagation dynamics.

Second and very important, just from the mathematics, it means that:

$$\begin{aligned}\chi^{(3)}(-\omega;\omega,-\omega,\omega) &= Re\chi^{(3)}(-\omega;\omega,-\omega,\omega) + iIm\chi^{(3)}(-\omega;\omega,-\omega,\omega) \\ &= \frac{4n_0^2\epsilon_0 c}{3}n_2 + i\frac{4n_0^2\epsilon_0 c}{3}\frac{c}{2\omega}\beta_{TPA}\end{aligned} \tag{2.20}$$

and thus

$$\frac{\omega}{c}n_2 + \frac{i}{2}\beta_{TPA} = \frac{3\omega}{4n_0^2\epsilon_0 c^2}\chi^{(3)}_{eff}(-\omega;\omega,-\omega,\omega) \tag{2.21}$$

where we have replaced $\chi^{(3)}$ by $\chi^{(3)}_{eff}$, which actually contain the symmetry information of silicon and the propagation and polarization direction of the wave (see [7, 8]). This tells us that though $\chi^{(3)}(-\omega;\omega,-\omega,\omega)$ cannot be directly measured, we can compute it since it is linked to the Kerr coefficient n_2 and the TPA coefficient β_{TPA} by a very simple relation. Measurements of β_{TPA} and n_2 have been performed by a number of researchers and though there are some discrepancies in the data actually obtained, we will be using some recent measurement results from Bristow et al [3], shown in Figure 2.7 below.

Though we will not consider the frequency dispersion of either n_2 or β_{TPA} in our work, it is instructive to look at the actual data of Figure 2.7. As expected, β_{TPA} decreases to essentially zero as we approach the midgap energy, that is $\lambda \sim 2.2\mu m$, and matches rather well with theoretical predictions. The Kerr coefficient n_2 however increases with wavelength and does not follow the Kramers-Krönig relation predicted from theory. The reason is because other contributions to n_2, namely the Raman and Stark effects contributions are not included.

2.2.3 Free Carrier effects

The TPA process described in the previous subsection leads to the generation of charge carriers in the waveguide. These carriers influence further propagation in two ways. First of all, they can absorb light at any wavelength,and this is the free carrier absorption. Second, they lead to a change in the refractive index and this has been called free

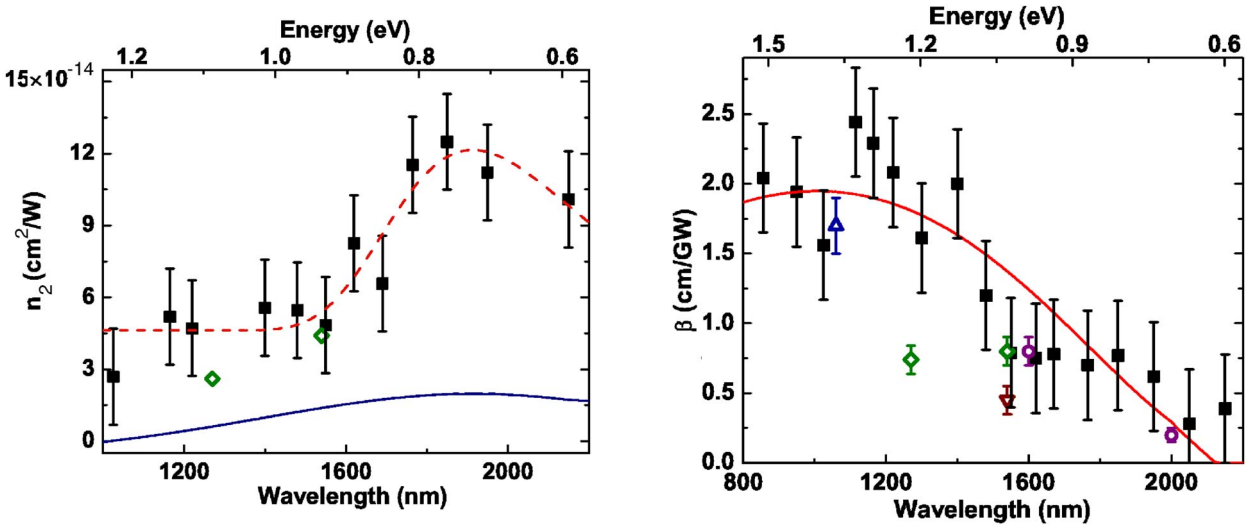

(a) (b)

Figure 2.7: (a) Measured values of n_2 (squares) as function of wavelength. Diamonds are data from Dinu et al. [5]. Solid line is Kramers-Krönig transformation of solid curve in b. (b) Measured values of β_{TPA} (squares) as a function of wavelength. Triangles and diamonds are data form other sources. Solid line is best theoretical fit. (After ref [3])

carrier dispersion. Because of their momentum relaxation times (average time required for the carrier to lose its original momentum due for example to a scattering event, given by $\tau = \frac{\mu m^*}{q}$) shorter than a ps, free carriers will be able to follow oscillations of the propagating wave almost instantaneously(see [8]). This leads to an additional polarization component that can be correctly described by the Drude model. The net result is a free carrier susceptibility given by:

$$\chi^f = 2n_0 \left[n_f + ic\alpha_f / 2\omega \right] \tag{2.22}$$

where n_f is the free carrier index change and α_f describes the free carrier absorption. They are given by [9]:

$$n_f = -\frac{q^2}{2\epsilon_0 n_0 \omega^2} \left(\frac{N}{m_e^*} + \frac{N^{0.8}}{m_h^*} \right) \tag{2.23}$$

$$\alpha_f = \frac{q^3 N}{\epsilon_0 c n_0 \omega^2} \left(\frac{1}{\mu_e m_e^*} + \frac{1}{\mu_h m_h^*} \right) \tag{2.24}$$

with q the electronic charge and μ the mobilities.

What's interesting in equations (2.23) and (2.24) is that both n_f and α_f will follow the time variation of the carrier concentration. This is very important as it can be used to monitor carrier dynamics in silicon waveguides.

Considering only generation through TPA and a carrier lifetime τ_c comprising both carrier drift and diffusion, the rate at which free carrier concentration changes can be derived as:

$$\frac{\partial N}{\partial t} = \frac{\beta_{TPA} I^2}{2\hbar\,\omega} - \frac{N}{\tau_c} \tag{2.25}$$

where I will be the intensity of the field inside the waveguide. This as we shall see, would allow us to incorporate all the effects described here into a model to describe pulse propagation inside the waveguide.

2.2.4 The Raman Response

As pointed out when describing the discrepancies between theory and the data of Figure 2.7, Raman scattering constitutes an additional third-order process in silicon. Raman scattering is that process which couples light and phonons, the net effect when two pulses with spectra separated by a Raman vibrational frequency co-propagate is the transfer of energy from one to the other. If it is however a monochromatic wave at frequency ω_p propagating alone, it will create a scattered stokes wave at ω_s downshifted from the pump signal by one Raman frequency, $\omega_R = \omega_p - \omega_s$. For silicon, the Raman response can be assimilated to a Lorentzian downshifted from the pump by $\omega_R/2\pi = 15.6THz$ with a spectral width $\Delta\omega/2\pi = 105GHz$.

Though the Raman response in silicon is very important and has been used to demonstrate lasing in silicon waveguides(see [6]), the Raman bandwidth is too narrow for the effect to be as significant as in fibres when short pulses propagate in Si waveguides. The formalism to include it when describing the dynamics of pulse propagation will follow along the same line, with the introduction of a Raman susceptibility tensor and Raman induced polarization. Again this becomes significant when two pulses separated by ω_R are copropagating, we then speak of stimulated Raman scattering. If the pulses are separated by less, they will interact via four-wave mixing, which is a $\chi^{(3)}$ effect.

2.3 Summary

We have seen both the linear and the relevant nonlinear optical process that may happen in Silicon in general. We have stressed the possibility silicon photonic wires offer to

engineer their dispersion characteristics, which is of paramount importance. The effects we have described in this chapter can be summarized in the figure below (from [10]).

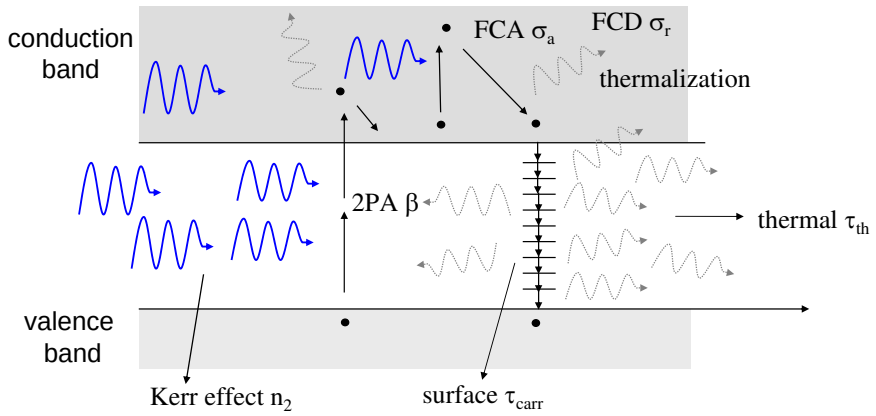

Figure 2.8: Summarizing nonlinear optical processes in silicon waveguides. As a strong light field enters the waveguide, it induces an intensity-dependent refractive index change: the Kerr effect. Two photons can be absorbed at the same time and this is TPA. Carriers generated by TPA can absorb light and induce a refractive index change, FCA and FCD. They also recombine, mostly at the surface as shown. These relaxations create phonons, will heat up the system.

These are the foundations we will use in the next chapter to build a model to understand how ultrashort pulses are affected as they propagate in a silicon waveguide, particularly how the interplay between dispersion and nonlinear effects can lead to significant spectral broadening.

Chapter 3

Theory of ultrashort pulse propagation in Silicon Photonic Wires.

We have in the previous chapter identified the major nonlinear effects in Si wires and defined nonlinear susceptibility tensors, along with the nonlinear polarization associated with each them. Here we provide a mathematical formulation of how these processes interact with each other and with waveguide dispersion to govern ultrashort pulse propagation inside the Si Wires.

3.1 Frequency domain propagation equation

Our starting point to develop the equation that governs pulse propagation inside the Si wires is the Maxwell wave equation, namely:

$$\vec{\nabla}^2 \vec{\mathbf{E}} - \frac{1}{c^2}\frac{\partial^2 \vec{\mathbf{E}}}{\partial t^2} = \mu_0 \frac{\partial^2 \vec{\mathbf{P}}}{\partial t^2} \tag{3.1}$$

where $\vec{\mathbf{P}}$ is the induced polarization in the propagation medium. We can write $\vec{\mathbf{P}}$ as linear and nonlinear components:

$$\vec{\mathbf{P}} = \vec{\mathbf{P}}_L + \vec{\mathbf{P}}_{NL} \tag{3.2}$$

The linear component $\vec{\mathbf{P}_L} = \epsilon_0 \chi^{(1)} \vec{\mathbf{E}}$ and we insert it in equation (3.1) to obtain:

$$\vec{\nabla}^2 \vec{\mathbf{E}} - \frac{1}{c^2}(1+\chi^{(1)})\frac{\partial^2 \vec{\mathbf{E}}}{\partial t^2} = \mu_0 \frac{\partial^2 \vec{\mathbf{P}}_{NL}}{\partial t^2} \tag{3.3}$$

Keeping in mind that $n_0^2 = 1 + \chi^{(1)}$ and transforming the previous equation to the frequency domain, we obtain:

$$\left[\overrightarrow{\nabla}^2 + \frac{\omega^2 n_0^2(\omega)}{c^2}\right]\widetilde{\mathbf{E}} = -\mu_0\omega^2\widetilde{\mathbf{P}}_{NL} \tag{3.4}$$

We now make a general assumption in that the nonlinear polarization resulting mainly from the third order nonlinearity and free carrier effects will be a perturbation to the linear wave equation and will not affect the modes of the waveguide. This generally holds, as the magnitude of the nonlinear effects is indeed very small. Under such assumption we write:

$$\widetilde{\mathbf{E}} = \widetilde{F}(x,y,\omega)\widetilde{\mathbf{A}}(z,\omega) \tag{3.5}$$

where $\widetilde{F}(x,y,\omega)$ governs the transverse mode profile(see for example Figure 2.3). Substituting $\widetilde{\mathbf{E}}$ in equation (3.4), we obtain:

$$\widetilde{\mathbf{A}}(z,\omega)\nabla_T^2\widetilde{F}(x,y,\omega) + \widetilde{F}(x,y,\omega)\frac{\partial^2}{\partial z^2}\widetilde{\mathbf{A}}(z,\omega) + \frac{\omega^2 n_0^2(\omega)}{c^2}\widetilde{F}(x,y,\omega)\widetilde{\mathbf{A}}(z,\omega) = -\mu_0\omega^2\widetilde{\mathbf{P}}_{NL} \tag{3.6}$$

We now multiply both sides of this equation by $\widetilde{F}^*(x,y,\omega)$ and integrate over the whole transverse plane to obtain :

$$\widetilde{\mathbf{A}}\iint \widetilde{F}^*\nabla_T^2\widetilde{F}dxdy + \frac{\partial^2}{\partial z^2}\widetilde{\mathbf{A}}\iint \left|\widetilde{F}\right|^2 dxdy + \widetilde{\mathbf{A}}\frac{\omega^2}{c^2}\iint \left|\widetilde{F}\right|^2 n_0^2(\omega)dxdy = -\mu_0\omega^2\iint \widetilde{F}^*\widetilde{\mathbf{P}}_{NL}dxdy \tag{3.7}$$

which we rewrite as:

$$\frac{\partial^2}{\partial z^2}\widetilde{\mathbf{A}}(z,\omega) + \beta^2(\omega)\widetilde{\mathbf{A}}(z,\omega) = -\mu_0\omega^2\frac{\iint \widetilde{F}^*\widetilde{\mathbf{P}}_{NL}dxdy}{\iint \left|\widetilde{F}\right|^2 dxdy} \tag{3.8}$$

where $\beta(\omega)$ is the propagation constant we introduced in the previous chapter and is given by :

$$\beta^2(\omega) = \frac{\frac{\omega^2}{c^2}\iint \left|\widetilde{F}\right|^2 n_0^2(\omega)dxdy + \iint \widetilde{F}^*\nabla_T^2\widetilde{F}dxdy}{\iint \left|\widetilde{F}\right|^2 dxdy} \tag{3.9}$$

The waveguide linear dispersion we described in the previous chapter and the plot of Figure 2.4 ($n_{eff}(\omega) = \frac{c}{\omega}\beta(\omega)$) are obtained from equation (3.9) after the modesolver

has computed the mode profile under the boundary conditions imposed by the waveguide geometry [8]. Indeed, waveguide geometry plays an extremely important role in determining its dispersive and even birefringence properties, this has been investigated in great detail by Daniel et al [12].

When no nonlinear polarization is induced, the solution of equation (3.8), which is then a simple Helmhlotz equation, will be of the form $e^{\pm i\beta(w)z}$. These are forward and backward propagating waves with constant transverse field distributions. Assuming that the field will propagate only in the forward $+z$ direction, we can use the slowly varying envelope approximation (SVEA):

$$\frac{\partial^2}{\partial z^2} + \beta^2(\omega) = \left(\frac{\partial}{\partial z} + i\beta(\omega)\right)\left(\frac{\partial}{\partial z} - i\beta(\omega)\right) \approx 2i\beta(\omega)\left(\frac{\partial}{\partial z} - i\beta(\omega)\right) \tag{3.10}$$

Equation (3.8) then becomes:

$$\frac{\partial}{\partial z}\widetilde{\mathbf{A}}(z,\omega) = i\beta(\omega)\widetilde{\mathbf{A}}(z,\omega) - \frac{\mu_0\omega^2}{2i\beta(\omega)}\frac{\iint \widetilde{F}^*\widetilde{\mathbf{P}}_{NL}dxdy}{\iint \left|\widetilde{F}\right|^2 dxdy} \tag{3.11}$$

We will now replace the nonlinear polarization $\widetilde{\mathbf{P}}_{NL}$ by the proper expression. We will consider mostly the free carrier and $\chi^{(3)}$ contributions. And thus:

$$\widetilde{\mathbf{P}}_{NL} = \widetilde{\mathbf{P}}^f + \widetilde{\mathbf{P}}^{(3)} \tag{3.12}$$

The third-order component is obtained from equation (2.9) as follows:

$$\widetilde{\mathbf{P}}^{(3)} = \frac{3}{4}\frac{1}{(2\pi)^2}\iiint d\omega_j d\omega_k d\omega_l \cdot \chi^{(3)}_{ijkl}(-\omega_i;\omega_j,-\omega_k,\omega_l)\widetilde{\mathbf{E}}(\mathbf{r},\omega_j)\widetilde{\mathbf{E}}^*(\mathbf{r},\omega_k)\widetilde{\mathbf{E}}(\mathbf{r},\omega_l) \tag{3.13}$$

where the factor $\frac{3}{4}$ accounts for the combinations of frequencies and we have explicitly expressed the nonlinear polarization (see [11]). As for the free carriers contribution, a calculation from the Drude model gives it in the time domain as follows:

$$\mathbf{P}^f(\mathbf{r},t) = \sum_{\omega_u}\left(N_e(\mathbf{r},t)\mathbf{p}^e(\omega_u) + N_h(\mathbf{r},t)\mathbf{p}^h(\omega_u)\right) \tag{3.14}$$

where $\mathbf{p}^\nu$ is the polarization response of a single carrier, obtained from the Drude model as $\mathbf{p}^\nu(\omega) = \epsilon_0\frac{q^2\tau_\nu}{\epsilon_0 m^*_\nu}\left(\frac{-1}{\omega(\omega\tau_\nu + i)}\right)\mathbf{E}(\omega,\mathbf{r},t)$. Thus, for a single frequency wave propagating in the waveguide, we can write in the frequency domain:

$$\widetilde{\mathbf{P}}^f(\mathbf{r},\omega) = \epsilon_0\chi^f(-\omega;\omega)\widetilde{\mathbf{E}}(\mathbf{r},\omega) \tag{3.15}$$

where $\chi^f(-\omega;\omega)$ is the free carrier susceptibility, and is obtained as:

$$\chi^f(-\omega,\omega) = \frac{q^2\tau_e}{\epsilon_0 m_e^*}\left(\frac{-1}{\omega(\omega\tau_e+i)}\right)\widetilde{N}_e(\mathbf{r},\omega) + \frac{q^2\tau_h}{\epsilon_0 m_h^*}\left(\frac{-1}{\omega(\omega\tau_h+i)}\right)\widetilde{N}_h(\mathbf{r},\omega) \quad (3.16)$$

. By separating the susceptibility in real and imaginary parts for free carrier and free carrier absorption, we arrive at equation (2.22).

We will now replace the electric fields in equations (3.13) and (3.15) by the expression (3.5), but first we normalize $\widetilde{\mathbf{A}}(z,\omega)$ such that its time domain counterpart has units of power, that is:

$$\widetilde{\mathbf{A}}(z,\omega) = \sqrt{\frac{2Z_0}{n}}\widetilde{\mathbf{a}} \quad (3.17)$$

Substituting all of this into equation (3.11) , we obtain the propagation equation below:

$$\begin{aligned}\frac{\partial}{\partial z}\widetilde{\mathbf{a}}(z,\omega) &= i\beta(\omega)\widetilde{\mathbf{a}}(z,\omega) + i\beta^f(-\omega;\omega)\widetilde{\mathbf{a}}(z,\omega) \quad (3.18)\\ &+ \iiint \gamma_{ijkl}(-\omega;\omega_j,-\omega_k,\omega_l)\widetilde{\mathbf{a}}(z,\omega_j)\widetilde{\mathbf{a}}^*(z,\omega_k)\widetilde{\mathbf{a}}(z,\omega_l)d\omega_j d\omega_k d\omega_l\end{aligned}$$

In the term representing the free carrier contribution, we have defined $\beta^f(-\omega;\omega)$ as :

$$\beta^f(-\omega;\omega) = \frac{\omega}{2n_{eff}(w)}\frac{\iint \chi^f(-\omega;\omega)\left|\widetilde{\mathbf{F}}(x,y,\omega)\right|^2 dxdy}{\iint \left|\widetilde{\mathbf{F}}(x,y,\omega)\right|^2 dxdy} \quad (3.19)$$

What this means, is remarkable. The net effect of free carriers will result from an overlap between carrier distribution and mode profile. This can be seen by noting that if χ^f is linear in carrier densities (that is ignoring the 0.8 power in equation (2.23), which is a valid approximation), then we have:

$$\beta^f(-\omega;\omega) = \frac{\omega}{2n_{eff}(\omega)}\chi^f(-\omega;\omega,\widetilde{\overline{\mathbf{N}}}); \text{ with } \widetilde{\overline{\mathbf{N}}} = \frac{\iint \widetilde{\mathbf{N}}\left|\widetilde{\mathbf{F}}(x,y,\omega)\right|^2 dxdy}{\iint \left|\widetilde{\mathbf{F}}(x,y,\omega)\right|^2 dxdy} \quad (3.20)$$

As the free carrier effects are linear in electric field, the expression for β^f can be further simplified since these effects will manifest themselves in the time domain mainly as a perturbation of the propagation constant(see [8]). By combining equations (3.20) and (2.22), we do obtain:

$$\beta^f(\omega,\overline{N}) = \frac{n_0(\omega)}{n_{eff}(\omega)}\left[\frac{\omega}{c}n_f + \frac{i}{2}\alpha_f\right] \quad (3.21)$$

It is now clear that both FCA and FCD will be significantly different in a waveguide when compared to bulk silicon. First of all there is an apparent enhancement factor that is the ratio between bulk and effective indices. Would the carrier density distribution be the same in bulk and in the waveguide, both FCA and FCD will be enhanced in the waveguide since n_{eff} is much smaller than the bulk index due to the confinement. Second, the average carriers density value used to compute FCA and FCD coefficients will be the one given by (3.20) which expresses the fact that only a fraction of the field will generate carriers and that they will interact with that fraction which is actually confined in the silicon waveguide. This, as pointed out in [7], is a direct consequence of the fact that only part of the mode actually overlaps with the silicon waveguide.

The last term in the propagation equation (3.18) governs the nonlinear processes we discussed in the previous chapter. The effective nonlinear coefficient is given by:

$$\gamma_{ijkl}(-\omega;\omega_j,-\omega_k,\omega_l) = \frac{3\omega\cdot\chi^{(3)}_{ijkl}(-\omega;\omega_j,-\omega_k,\omega_l)}{4\epsilon_0 c^2(n_\omega n_j n_k n_l)^{\frac{1}{2}}}\frac{\iint \widetilde{F}^*_\omega \widetilde{F}_j \widetilde{F}^*_k \widetilde{F}_l dxdy}{\prod\limits_{\nu=\omega,j,k,l}\left[\iint\left|\widetilde{F}_\nu\right|^2 dxdy\right]^{\frac{1}{2}}} \tag{3.22}$$

We can simplify this expression by writing it as:

$$\gamma_{ijkl}(-\omega;\omega_j,-\omega_k,\omega_l) = \frac{3\omega\eta_{\omega jkl}}{4\epsilon_0 c^2\overline{a}(n_\omega n_j n_k n_l)^{\frac{1}{2}}}\cdot\chi^{(3)}_{ijkl}(-\omega;\omega_j,-\omega_k,\omega_l) \tag{3.23}$$

where we have defined the mode-overlapping factor:

$$\eta_{\omega jkl} = \frac{\iint \widetilde{F}^*_\omega \widetilde{F}_j \widetilde{F}^*_k \widetilde{F}_l dxdy}{\prod\limits_{\nu=\omega,j,k,l}\left[\iint\left|\widetilde{F}_\nu\right|^4 dxdy\right]^{\frac{1}{4}}} \tag{3.24}$$

and the average effective mode area as:

$$\overline{a} = (a_\omega a_j a_k a_l)^{\frac{1}{4}},\ \text{with}\ a_\nu = \frac{\left[\iint\left|\widetilde{F}_\nu\right|^2 dxdy\right]^2}{\iint\left|\widetilde{F}_\nu\right|^4 dxdy} \tag{3.25}$$

Equations (3.22) – (3.25) show once again that the effective nonlinear coefficient is very dependent on the waveguide geometry and the overlap between the modes of the waves that interact via the nonlinearity. If we have only one wave centered at frequency

ω, the nonlinear parameter simplifies into the same expression that is used for fibers (see Agrawal). This allows us first to outline the flaws in our approach that will lead to inaccuracies. We have made two assumptions that are not true for Si photonic wires. In reaching Eq. (3.22) we have assumed that the susceptibility $\chi^{(3)}$ has no spacial dependence, and we have also ignored the spacial dependence of the dielectric constant when starting with the Maxwell wave equation (that is, we've assumed $\nabla \cdot \mathbf{D} = \epsilon \nabla \cdot \mathbf{E} = 0$), all of which is not accurate. Second, we have assumed that the field will have negligible longitudinal component and have ignored the vectorial nature of $\widetilde{\mathbf{F}}(x, y, \omega)$. Though this is generally true for the case of low contrast waveguides such as optical fibers, it does not hold for high contrast structures such as the Si photonic wires. While still assuming $\chi^{(3)}$ constant over the cross-section of the waveguide core and zero outside, we can adjust our definition of the effective area to correct for some of the accuracy. We will therefore adopt the definition of Koos et al [13], which is:

$$a_{eff} = \frac{Z_0^2}{n_{Si}^2} \frac{\left| \iint_{A_\infty} Re\left[\mathcal{E}_\mu(x,y,\omega) \times \mathcal{H}_\mu^*(x,y,\omega)\right] \cdot \mathbf{e}_z dxdy \right|^2}{\iint_{A_0} \left|\mathcal{E}_\mu(x,y,\omega)\right|^4 dxdy} \tag{3.26}$$

where $\mathcal{E}_\mu(x, y, \omega)$ and $\mathcal{H}_\mu(x, y, \omega)$ are the vectorial electric and magnetic mode profiles (similar to $\widetilde{\mathbf{F}}$) for the mode μ of the waveguide. A_∞ is the cross section of the whole structure while A_0 is the cross section of the silicon core. With this definition, we will have the effective nonlinear coefficient for a single wave at ω defined as:

$$\gamma = \frac{3\omega}{4\epsilon_0 c^2 n_{Si}^2 a_{eff}} \cdot \chi^{(3)}(-\omega; \omega, -\omega, \omega) \tag{3.27}$$

With this adjustment, the general propagation equation (3.18) is similar to that developed by Osgood et al, which can be found in [1, 7, 13].This equation is quite general since it contains all the dispersive, nonlinear and free carrier effects. It contains also the frequency dispersion of all the nonlinear parameters, though as we said earlier, we would ignore it in modeling since we assume that both free carriers and third order susceptibility doesn't change much across the spectrum of a single pulse. The linear scattering losses at sidewall roughness can be included in a straightforward manner using an attenuation coefficient. Together with equation (2.25), which we rewrite as:

$$\frac{\partial N}{\partial t} = \frac{\beta_{TPA}}{2\hbar\,\omega a_{eff}^2} \left|\mathbf{a}(z,t)\right|^4 - \frac{N}{\tau_c} \tag{3.28}$$

this completes the formulation of nonlinear pulse propagation in Si photonic wires. It is however, instructive to transfer this equation to the time domain where more insight can be actually gained as to the physical processes that affect pulse propagation.

3.2 Time domain Formalism

Throughout the present work, the wave we use to interrogate the waveguide is in a form of a pulse train. These pulses are centered around the carrier frequency $\omega_0 = \frac{2\pi c}{\lambda_0}$, with $\lambda_0 = 1.55\mu m$. We will therefore replace the propagation constant $\beta(\omega)$ by a Taylor series around ω_0, and to get the time domain equivalent of equation (3.18) , we replace $\omega - \omega_0$ with a time derivative $i\frac{\partial}{\partial t}$. We therefore obtain:

$$\frac{\partial a}{\partial z} = i\sum_{m=0}^{m=\infty} i^m \beta_m \frac{\partial^m a}{\partial t^m} + i\beta^f(\omega_0, \overline{N})a + i\left(1 + i\xi\frac{\partial}{\partial t}\right)P^{NL}(z,t) \tag{3.29}$$

where the nonlinear polarization can be replaced by its time domain form [8, 14, 11]:

$$P^{NL}(z,t) = a_j(z,t)\int_{-\infty}^{\infty} \mathbf{R}^{(3)}(t-\tau)a_k^*(z,\tau)a_l(z,\tau)d\tau \tag{3.30}$$

The response function as we will take it, is simply:

$$\mathbf{R}(t) = \gamma_{eff}^e \delta(t) + \gamma_{eff}^R h_R(t) \tag{3.31}$$

where the Raman and electronic contributions have been made very explicit. The dirac delta symbolizes the fact that bound electronic response is almost instantaneous, while the Raman response $h_R(t)$ is delayed. We obtain it by looking at the Raman spectrum for silicon. We mentioned in the previous chapter that the Raman response for silicon would be a Lorentzian shifted from the pump by $\frac{\omega_R}{2\pi} = 15.6THz$ and with a bandwidth $\frac{\Delta\omega_R}{\pi} \approx 105GHz$. The frequency domain response is therefore:

$$\widetilde{H}_R(\omega) = \frac{\omega_R^2}{\omega_R^2 - \omega^2 - 2i\omega\Delta\omega_R} \tag{3.32}$$

Taking the inverse Fourier transform of this expression, we end up with:

$$h_R(t) = \omega_R^2 \tau_1 \sin(t/\tau_1)e^{-t/\tau_2} \times U(t) \tag{3.33}$$

where $\tau_2 = 1/\Delta\omega_R \approx 3ps$ is the optical phonon lifetime, $\tau_1 = 1/(\omega_R^2 - \Delta\omega_R^2)^{1/2} \approx 1/\omega_R \approx 10fs$, and $U(t)$ is the heaviside step function.

The Raman nonlinear parameter appearing in equation (3.31) depends on the Raman gain as:

$$\gamma_{eff}^{R}(\omega_0) = \frac{g_R \Delta\omega_R}{a_{eff}\omega_R} \tag{3.34}$$

Now the Raman gain g_R has been widely investigated and its value measured in either spontaneous or stimulated Raman scattering experiments (see [15, 16]). Despite the very high gain value (4 to 76 cm/GW), the nonlinear parameter depends on $\Delta\omega_R/\omega_R$ and will end up contributing very little to the nonlinearities. Furthermore, the input pulse spectrum has to be wide enough for the Raman response to be significant. The Raman contribution can be characterized by a factor f_R defined as:

$$f_R = \frac{\gamma_{eff}^{R}}{\gamma_{eff}} \tag{3.35}$$

where γ is the total nonlinear parameter. From Raman gain measurements and both n_2 and β_{TPA} data available in literature, $f_R \approx 0.043$. We therefore rewrite the Response function as:

$$R(t) = \gamma_{eff}\left[(1 - f_R)\delta(t) + f_R h(t)\right] \tag{3.36}$$

and γ_{eff} can take the very simple form also used in fibers by combining equations (3.27) and (2.21):

$$\gamma_{eff} = \frac{\omega n_2}{c a_{eff}} + i\frac{\beta_{TPA}}{2a_{eff}} \tag{3.37}$$

Finally, ξ appearing in the time domain propagation equation (3.29) is responsible for two other effects worth mentioning, namely self-steepening and shock formation. Self-steepening refers to the distortion a pulse would undergo as a result of its group velocity being dependent on its peak power. Conceptually, if the refractive index is to be dependent on intensity, then for a pulse, different temporal components would feel different indices of refraction. Therefore, the shift in the group velocity would be dependent on the local pulse power. Ultimately, ξ takes root in the frequency dependence of the nonlinear parameter. Its value is obtained from(see [8, 7]):

$$\xi = \frac{\partial}{\partial\omega} ln(\gamma(\omega))\Big|_{\omega_0} = \frac{1}{\omega_0} - \frac{1}{a_{eff}}\frac{\partial a_{eff}}{\partial\omega}\Big|_{\omega_0} + \frac{1}{\chi_{eff}^{(3)}}\frac{\partial\chi_{eff}^{(3)}}{\partial\omega}\Big|_{\omega_0} \tag{3.38}$$

Self-steepening has been extensively studied in optical fibers where it is custom to characterize it with a shock time τ_s defined the same way we defined the parameter ξ here. While for fibers the last two terms can be neglected on the grounds that both n_2 and a_{eff} have negligible dispersion, it is not absolutely true for Si photonic wires. Osgood et al. [7] have shown through numerical calculations that for Si photonic wires, $\tau_s = \xi$ can be as large as $25fs$ with considerable imaginary part. But again, the effect is more significant only when the input spectrum is quite broad as is the case in continuum generation. We will however, neglect the last two terms in our numerical studies.

We will now replace $a(z,t)$ in equation (3.29) with $a(z,t)e^{i\beta_0 z}$ and then shift the time frame by $T = t - \beta_1 z$ so that the pulse center always corresponds to $T = 0$. If we now just consider a single pulse centered around ω_0, we can resume the propagation equations as follows:

$$\frac{\partial a}{\partial z} = -\frac{\alpha}{2}a + i\sum_{m=2}^{m=\infty}\frac{i^m\beta_m}{m!}\frac{\partial^m a}{\partial T^m} + i\beta^f(\omega_0,\overline{N})a \quad + \quad i\gamma_{eff}\left(1 + i\tau_s\frac{\partial}{\partial T}\right)a(z,T)\times \int_{-\infty}^{\infty} R(T-\tau)\left|a(z,\tau)\right|^2 d\tau \tag{3.39}$$

$$\frac{\partial \overline{N}}{\partial t} = \frac{\beta_{TPA}}{2\hbar\,\omega a_{eff}^2}\left|\mathbf{a}(z,t)\right|^4 - \frac{\overline{N}}{\tau_c} \tag{3.40}$$

These are the coupled equations that we will use to numerically investigate nonlinear pulse propagation in Si photonic wires. The first one is the famous generalised nonlinear Schrödinger equation. Again, it is quite general and we will make some simplifications when trying to simulate only certain precesses.

3.3 Numerical solution to the Propagation equation

The propagation equation we just arrived to is quite complex, and it's usually impossible to solve it analytically if no significant simplifications are made. There have been however, many numerical techniques which allow to obtain a solution. The split-step fourier method does just that, and what we will use in our approach is more or less the same. But first, we rewrite the propagation equation in a more suitable form, so that it would be easier to actually implement a numerical solution.

Taking the Fourier transform of equation (3.39) and with the notation $\widetilde{A}(z,\omega) = \mathcal{F}\left[a(z,t)\right]$ we obtain:

$$\frac{\partial \widetilde{A}(z,\omega)}{\partial z} = -\frac{\alpha}{2}\widetilde{A}(z,\omega) + i\sum_{m=2}^{m=\infty}\beta_m\frac{(\omega-\omega_0)^m}{m!}\widetilde{A}(z,\omega) + \mathcal{F}\left\{ i\beta^f(\omega_0,\overline{N})a + i\gamma_{eff}\left(1+i\tau_s\frac{\partial}{\partial T}\right)a(z,T)\int_{-\infty}^{\infty}R(T-\tau)\left|a(z,\tau)\right|^2 d\tau \right\} \tag{3.41}$$

Where we have explicitly separated the linear part, that is dispersion and linear loss, and the nonlinear part. It is obvious that when required, dispersion to all orders will be included simply by noting that:

$$\sum_{m=2}^{m=\infty}\beta_m\frac{(\omega-\omega_0)^m}{m!}\widetilde{A}(z,\omega) = \left[\beta(\omega)-\beta(\omega_0)-\beta_1(\omega_0)\cdot(\omega-\omega_0)\right]\widetilde{A}(z,\omega) \tag{3.42}$$

To move forward, we will define the linear operator as:

$$\hat{L} = i\frac{\alpha}{2} + \sum_{m=2}^{m=\infty}\beta_m\frac{(\omega-\omega_0)^m}{m!} \tag{3.43}$$

This leads us to rewrite the previous equation as:

$$\frac{\partial \widetilde{A}}{\partial z} = i\hat{L}\widetilde{A} + \mathcal{F}\left[i\beta^f(\omega_0,\overline{N})a + i\gamma_{eff}\left(1+i\tau_s\frac{\partial}{\partial T}\right)a(z,t)\int_{-\infty}^{\infty}R(T-\tau)\left|a(z,\tau)\right|^2 d\tau \right] \tag{3.44}$$

we will now make a change of variable as follows:

$$\widetilde{\mathcal{A}} = \widetilde{A}(z,\omega)e^{-i\hat{L}z} \tag{3.45}$$

This allows us to get rid of the first term on the right, and the equation to solve becomes:

$$\frac{\partial \widetilde{\mathcal{A}}}{\partial z} = e^{-i\hat{L}z}\times\mathcal{F}\left[i\beta^f(\omega_0,\overline{N})a + i\gamma_{eff}\left(1+i\tau_s\frac{\partial}{\partial T}\right)a(z,t)\int_{-\infty}^{\infty}R(T-\tau)\left|a(z,\tau)\right|^2 d\tau \right] \tag{3.46}$$

taking $\tau_s = 1/\omega_0$, this leads to:

$$\frac{\partial \widetilde{\mathcal{A}}}{\partial z} = e^{-i\hat{L}z}\left\{ \mathcal{F}\left[i\beta^f(\omega_0,\overline{N})a(z,t)\right] + i\gamma_{eff}\frac{\omega}{\omega_0}\mathcal{F}\left[a(z,t)\int_{-\infty}^{\infty}R(T-\tau)\left|a(z,\tau)\right|^2 d\tau \right] \right\} \tag{3.47}$$

Again, we have assumed the nonlinear parameter does not change with frequency. What we have reached here is remarkable in that this equation is an ordinary differential equation, as we have gotten rid of the stiff dispersive part. This means that we can readily implement it using ODE tools available in MATLAB. This change of variable to transform the GNLSE into an ODE were first suggested by Caradoc-Davies in his work on Bose-Einstein condensates where an equation similar to the GNLSE has to be solved. He went on to develop what he called a fourth order Runge-Kutta algorithm in the interaction picture (see [17]). This method was adapted to simulate continuum generation in fibers by Hult [18] and others. John Dudley et al. [19] generalized the approach, exploiting MATLAB's ODE tools, to make a wide range of simulations for an extensive review of continuum generation. The method is more efficient in that the number of Fourier transform steps is reduced when compared to standard split-step algorithms, while preserving an accuracy of the order of $0(\Delta z^4)$, where Δz is the propagation step.

We started our modeling work from a simulation code in the recently published book by Dudley and Taylor [20]. Stéphane Coen kindly provided us with that code while the book was still unpublished.

From equation (3.47), it is obvious however, that dealing with Si photonic wires will be different from optical fibers. This is mostly because of the free carriers effects, since TPA can be simply included as an imaginary part to the effective nonlinear coefficient. We have to compute the carrier concentration $\overline{N}$ after each propagation step so as to update the value of β^f. This forces us to create a loop, doubling the number of Fourier transform and the net result is a penalty in efficiency and speed.

The algorithm to implement the solution to the propagation equation can be summed up as follows:

1. Compute the right hand side of equation (3.47)

2. Propagate through one step Δz, by solving the equation in the Fourier domain. We make use of MATLAB's *ode*45 solver to achieve this and one ends up with $\widetilde{\mathcal{A}}(z+\Delta z,\omega)$. *ode*45 itself, is an algorithm based on the Runge-Kutta method.

3. Save the above result and then transform back to the time domain by performing

$$a(z+\Delta z,T)=\mathcal{F}^{-1}\left[e^{i\hat{L}z}\widetilde{\mathcal{A}}(z+\Delta z,\omega)\right] \tag{3.48}$$

4. Compute the free carrier concentration as a function of time T from equation (3.40). Then update the value of β^f, which of course will be a function of time.

5. Go back to step 1 and start the process all over. At the end, the stored value of $\widetilde{\mathcal{A}}(z,\omega)$ are retrieved and the spectral domain solution obtained by reversing the change of variable made earlier.

Correct implementation of this algorithm in MATLAB has allowed us to model pulse propagation in Si wire waveguides, and built an understanding of the processes we discuss in the next chapter.

3.4 Model Validation

To validate our model, we run simulations based on data and parameters found in two widely cited articles. The first is a paper from L. Yin et al [22] of the Institute of Optics, Rochester. The authors demonstrate by numerically solving the GNLSE that continuum generation can occur in silicon waveguides through soliton fission and dispersive wave generation. Figure 3.1 shows their numerical results on the left, and those we obtained from our own modeling on the right. In their work, a $50fs$ pulse centered at $1550nm$ and having a peak power of $25W$ is launched in a $0.7 \times 0.8\mu m^2$ Si wire. Such a wire has a zero dispersion wavelength at $1492nm$, and its parameter were chosen so that the $sech^2$ pulse would behave as a third order soliton. Propagation in $1.2cm$ long waveguide results in the soliton breaking down in its fundamental constituents, with the emission due to third-order dispersion of a dispersive wave at the back of the pulse.

The result in the time domain is a tremendous spectral broadening, with the output spectrum stretching from about 1.3 to $1.7\mu m$. To a good approximation, our results are the same as theirs. The slight differences are due to the fact that we have not incorporated dispersion beyond the third order, and have taken a loss value of $1.2dB/cm$ as no value is given in the article. This loss value is relatively low, but for large waveguides such as the $0.7 \times 0.8\mu m^2$, it is reasonable. Simulations with higher values also give the very same effects.

The second example is from a recent review by Osgood et al. [7]. We propagate a $100fs$ pulse of $6.5W$ peak power in a $360 \times 220nm^2$ waveguide. Such a waveguide has its second ZDW at $1550nm$, but the input pulse is centered at $1500nm$ so that we are in the anomalous dispersion regime. The figure below shows comparison between their modeling results and ours for the same parameters. We have made a color plot of the evolution of both the temporal and spectral profile along the waveguide length.

In part (a), TPA and free carriers effects are ignored, and thus we have the same dynamics as in fibers. Huge spectral broadening happens only over $1cm$ of propagation

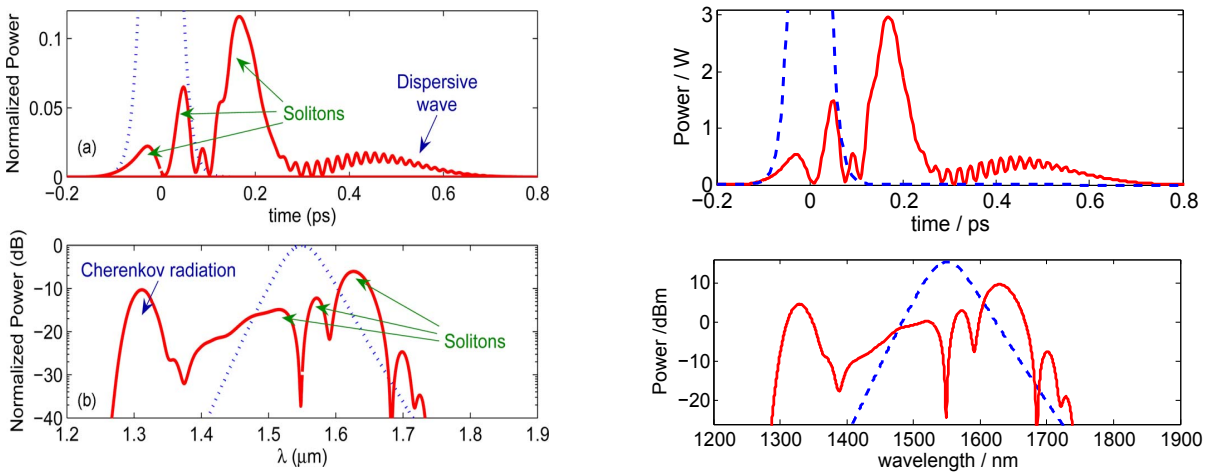

(a) (b)

Figure 3.1: Soliton fission and supercontinuum generation in silicon photonic wires. (a) Numerical results as taken from reference [22] (b) Numerical results from our own implementation of equation (3.47).In both (a) and (b), the top figure represents the temporal profile of both the input pulse (blue dashed curve) and output pulse (red curve). The bottom curves show input(blue dashed curve) and output(red) spectra.

with very low peak power, and this is due to the large nonlinear coefficient of silicon as well as the small dimensions of the waveguide. After just $1mm$, the pulse splits into two solitons which group velocity are slightly larger than that of the input pulse. In part(b), we ignore TPA while nevertheless adding the effects of TPA-generated free carriers. We see that the soliton with higher peak power soliton is accelerated under the influence of free carrier dispersion. In part (c), a full simulation including all the effects is carried out, and we can see that the effects of free carriers are no so important anymore. This can be understood by realizing that, with TPA included, the nonlinear loss becomes significant and so carrier densities are reduced along the propagation distance. Our simulation results compares well with theirs and all the the major effects that affect pulse propagation are portrayed. There are disparities however, which are due once again to the linear loss value we chose, but mainly to the fact that the propagation equation Osgood et al. use in their modeling is slightly different from ours. They start from the Lorentz reciprocity theorem and rigorously compute the effective susceptibilities for the waveguide. Nevertheless, the similarity between our results and theirs is striking.

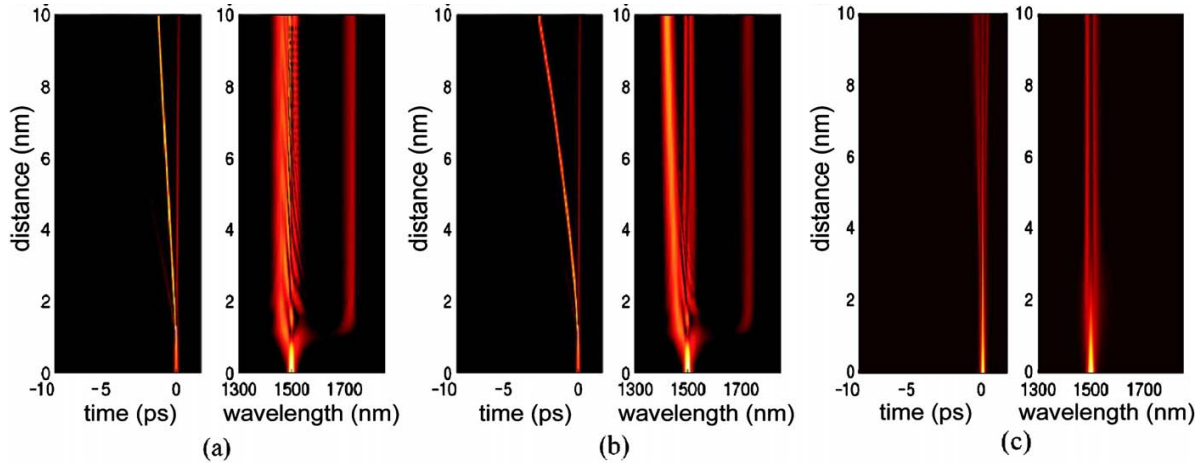

(A)

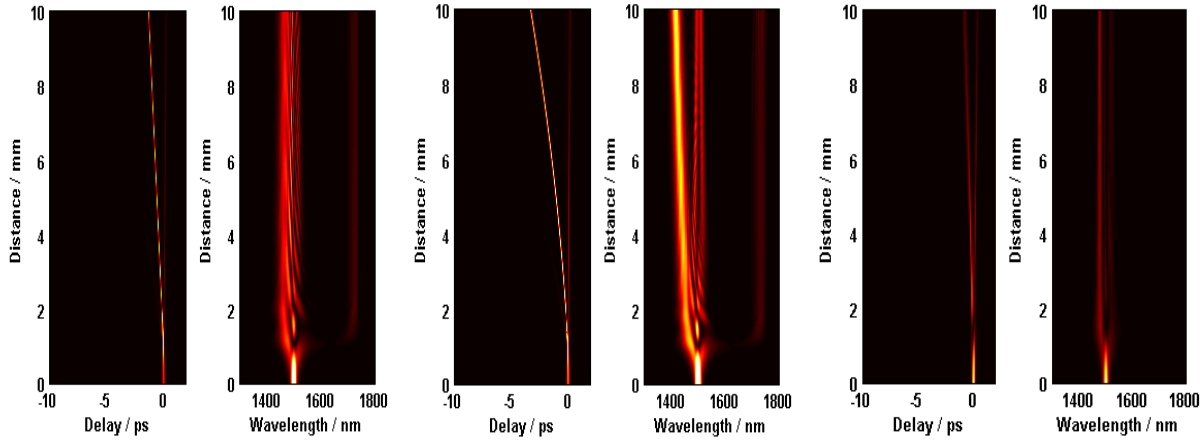

(B)

Figure 3.2: Propagation of a pulse with $T_0 = 100fs$, peak power $P_0 = 6.5W$, and pulse wavelength $\lambda = 1500nm$ in a SPW with dimensions $w \times h = 360 \times 220nm^2$, for which the ZGVD wavelength $\lambda_0 = 1550nm$, $\beta_2 = -4ps^2/m$,$\beta_3 = -0.0915ps^3/m$, and $\gamma = 446.5W^{-1}m^{-1}$. Top subfigure (A) is from the article [7] and bottom one (B) is from our own work. In both cases: (a) Influences of the TPA and free carriers are neglected; (b) influence of TPA is ignored while free carriers effects are included; (c) both TPA and free carriers are fully accounted for.

3.5 Summary

We have provided a theoretical background and developed a description of pulse propagation in SPWs starting from Maxwell's equation. We have then introduced a numerical model to solve the nonlinear propagation equation, and it compares very well with what can be found in literature. As the present work is more experimental than theoretical, our intent and interest in numerical modeling is to get a guideline as to what to expect as outcome of experiments. Modeling also offers great insight as to how to interpret the outcome of experiments. We devote the next chapter to a number of simulations with both waveguide and pulse parameters available for us in the lab.

Chapter 4

Dynamics of continuum generation in Si photonic wires

Continuum generation, arguably one of the most spectacular achievements of nonlinear optics, results from a cascade of nonlinear processes that occur as a strong pulse of light propagates in a nonlinear medium. The physics behind it can be very different depending on pulse parameters such as initial peak power, pulsewidth and pulse shape as well as waveguide parameters such as effective nonlinearities, dispersion and waveguide length. Because of that, there is no unified theory that can equally well explain the outcome of all supercontinuum generation experiments, be it in fibers or as in our case, in Si photonic wires. In this chapter, we aim to provide a description of some of the major effects in Si photonic wires that lead to spectral broadening, illustrating each case with simulations results from our modeling. The parameters are selected from those available to us in the lab after simple calculations based on the theory we developed in the previous chapter.

4.1 Relative Importance of nonlinear and dispersive effects in Si photonic wires.

We have made clear in the previous chapter that pulse propagation in Si photonic wires will be governed by an interplay between dispersive and nonlinear effects. To characterize the importance of one or the other, characteristic lengths are often adopted. The dispersion length (GVD length) is defined as $L_D = \frac{T_0^2}{|\beta_2|}$, the third order dispersion length

as $L_D^{'} = \frac{T_0^3}{|\beta_3|}$, with T_0 being the pulsewidth. The nonlinear length is $L_{NL} = \frac{1}{\gamma_{eff} P_0}$. If we consider a $w \times h = 450 \times 220nm^2$, the characteristics lengths are shown in the table below for $1.2ps$ and $212fs$ pulses.

We can readily see that for picosecond pulses with $P_0 = 1W$ or larger, $L_{NL}/L_D \ll 1$ and $L_{NL}/L_D^{'} \ll 1$. The dispersive effects can therefore be ignored. We stress out here once again that, due to the method we used to obtain third-order dispersion coefficients,i.e, by successive derivatives of the propagation constant, there is a considerable uncertainty in the results we obtain. For example, while our results in table 4.1 agree well with the data from Osgood et al. [7] for GVD length, there are some disparities for TOD lengths. Nevertheless, the conclusion we are able to reach based on this data is rather accurate.

For femtosecond pulses however, these lengths become comparable and also approach the typical propagation length of $1cm$. Dispersion then has to be fully accounted for. It is custom to define the parameter N called the soliton number, $N = \left(\frac{L_D}{L_{NL}}\right)^2$, which describes the strength of solitonic effects. This is relevant only when we are in the anomalous GVD regime.

4.2 Self-phase modulation in SPWs

Self-phase modulation is the most fundamental mechanism that leads to the spectral broadening of a short pulse. It is intuitively understood by considering the kerr effect. If the refractive index changes with the local intensity, then as a pulse propagate, it will undergo a time dependent phase change that is related to the temporal profile of the pulse. Such a time dependent phase change is indeed equivalent to frequency shift.

In SPWs, as opposed to fibres for example, TPA-generated free carriers will significantly impact SPM. To see this we run simulations with and without TPA and FCA as

Table 4.1: Characteristic lengths for a $450 \times 220nm^2$ waveguide

Characteristic Length	$T_0 = 1.2ps$	$T_0 = 212fs$
L_D	$26.5cm$	$1.1cm$
$L_D^{'}$	$107.6m$	$0.96m$
L_{NL} for $P_0 = 1W$	$2.3mm$	$2.3mm$

well as FCD. Our basic assumption is that the repetition rate is low enough ($\leq 500MHz$) for carriers generated by one pulse to completely recombine before the next pulse comes in, the so called single pulse approximation. Under this approximation, the propagation equation reduces to:

$$\frac{\partial a(z,T)}{\partial z} = -\frac{\alpha}{2}a - i\frac{\beta_2}{2}\frac{\partial^2 a}{\partial T^2} + \frac{\beta_3}{6}\frac{\partial^3 a}{\partial T^3} + i\beta^f(\omega_0, \overline{N})a + i\gamma_{eff}\left|a\right|^2 a \tag{4.1}$$

Figure 4.1 shows self-phase modulation of a picosecond pulse as it propagates in a SPW. We have included dispersion and it can be seen on the density plot that, second order dispersion leads indeed to temporal pulse compression. The effects of TPA and free carrier effects can be readily seen. TPA severely reduces the extent of broadening, and this is intuitive in that, as nonlinear loss due to TPA is introduced, the pulse peak power decreases and so does the phase change associated with SPM. The SPM spectrum is also symmetric with respect to the reference wavelength, however, this ceases to be the case when free carrier effects are introduced. FCA causes the little decrease in amplitude, while FCD cause a slight shift towards shorter wavelengths, thus creating the asymmetry. Whereas the kerr effect creates blue-shifted frequencies on the trailing edge of the pulse and red-shifted ones on the leading edge, FCD induces a blue shift at

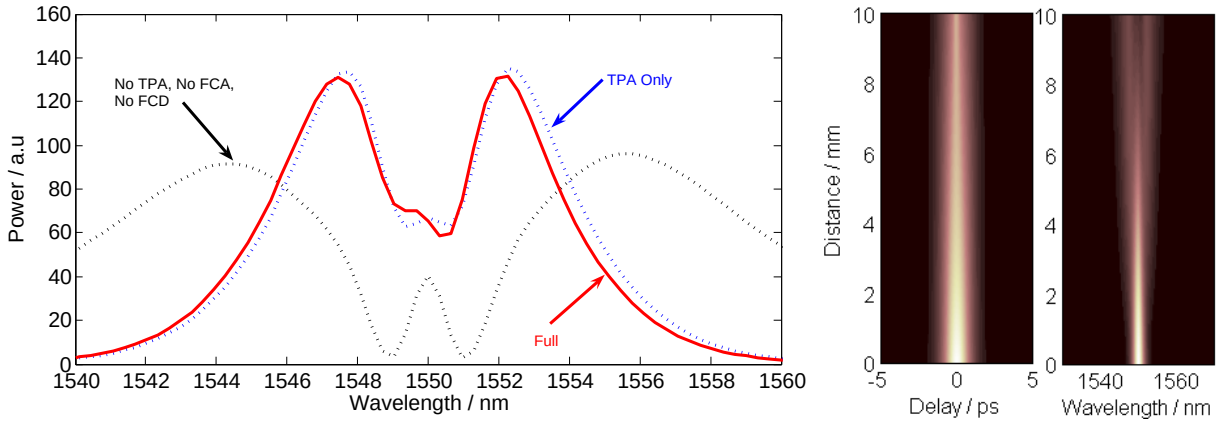

(A) (B)

Figure 4.1: Self-phase modulation in a $450 \times 220nm^2$, $1cm$ long silicon photonic wire. We propagate a pulse with $T_0 = 1.2\ ps$, $P_0 = 1.3W$ in the SPW. In (A), we show the output spectrum when no TPA, nor free carrier effects are considered, then TPA only is considered and finally all the effects are incorporated. In (B), we show the temporal and spectral evolution along the waveguide length when all the effects are included.

both edges. FCD thus counteract the kerr effect on the leading edge, while both add up on the lagging edge and thus the asymmetry. This is in agreement with experimental results from Dulkeith et al [24], and also numerical results from Yin et al. [23].

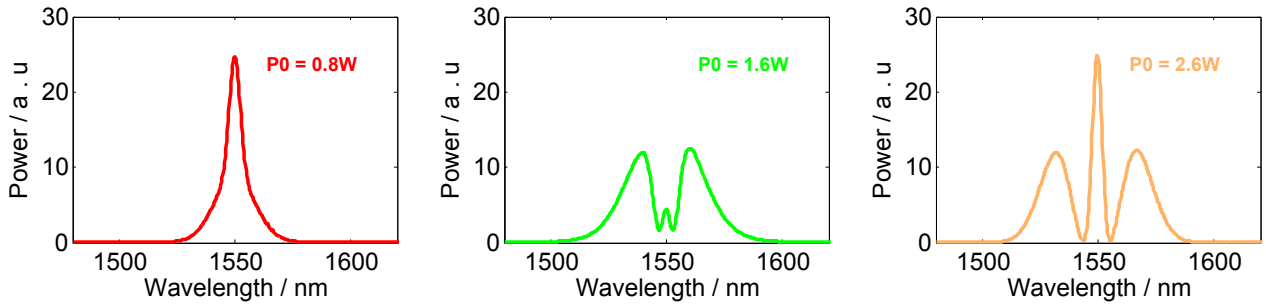

(A) No Third-order dispersion

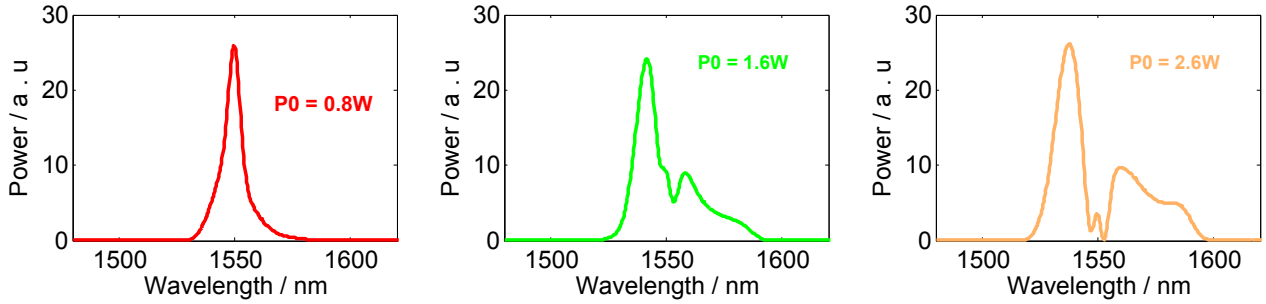

(B) Third-order dispersion included

Figure 4.2: Self-phase Modulation in a $450 \times 220nm^2$, $5mm$ long silicon photonic wire. We propagate a pulse with $T_0 = 200\ fs$, with the shown peak powers in the SPW. In (A), output spectra are recorded when third order dispersion is totally ignored. In (B), we include TOD and the asymmetry of the SPM spectra is obvious. Carrier effects and TPA are fully incorporated in both cases. Third order dispersion data is taken from [25].

In the case of femtosecond pulses however, SPM is strongly affected not by free carrier effects, but by third-order dispersion, as has been shown by Hsieh et al. [25]. Figure 4.2 illustrates this point. Using $\beta_3 = -0.73 ps^3/m$ from their work, we show here that third order dispersion indeed distorts the SPM spectrum. TOD distorted spectra are in perfect agreement with their experimental results.

The power levels and propagation lengths required to observe SPM in Si photonic

wires are orders of magnitude less those for fibers. In reference [25], the authors claim that spectra similar to the above figure are obtained with input peak powers from 50 to 250mW. Both our numerical and experimental results suggest otherwise. In SPWs with $450 \times 220nm^2$ cross section, these figures should be increased by at least one order of magnitude.

In supercontinuum generation, self-phase modulation almost always initialize the broadening process. Cross-phase modulation, which implies that a pulse will feel the nonlinear index of another one when co-propagating, can be also important. This is the case for example in fibres where XPM can be important in flattening the continuum (see Dudley et al., [19]). XPM switching has been observed in Si waveguides with larger dimensions(see [27]), around $2\mu m$, and can be numerically studied using coupled-mode theory. That is, using our development in the previous chapter for the case where two pulses at different wavelengths are present. We do not concern ourselves with such a study in this work.

When treating SPM, it is custom to ignore dispersion. As we showed in Figures 4.1 and 4.2 however, the interplay between the two leads to interesting effects. In the normal GVD regime, we will have simultaneous temporal and spectral broadening. In the anomalous GVD regime however, this can lead to the creation of solitons. For optimum spectral broadening, pumping should be done in this regime. To show why, we run a simulation with a $1.2ps$ pulse, but this time with its peak power increased to $P_0 = 10W$. The results are shown in Figure 4.3. In one case, we include all the effects and use the proper sign for the GVD coefficient, which for the $450 \times 220nm^2$ is in the anomalous regime. After propagation over $1cm$, the pulse in the time domain is very much distorted, and breaks down into shorter pulses. The output spectrum is many times broader than at the input. When we reverse the sign of β_2 but keep everything unchanged, we witness a simple temporal broadening of the pulse, along with a spectral response that shows the spectral modulation which is signature of SPM.

Pumping SPWs in the anomalous GVD regime thus allows for soliton-like features to appear, and thus optimizing the broadening. We next focus on the description of such features.

4.3 Soliton dynamics in SPW

In the anomalous GVD regime, the nonlinear chirp that results from SPM and the linear chirp from β_2 can combine in such a way that they cancel each other and yield a stable

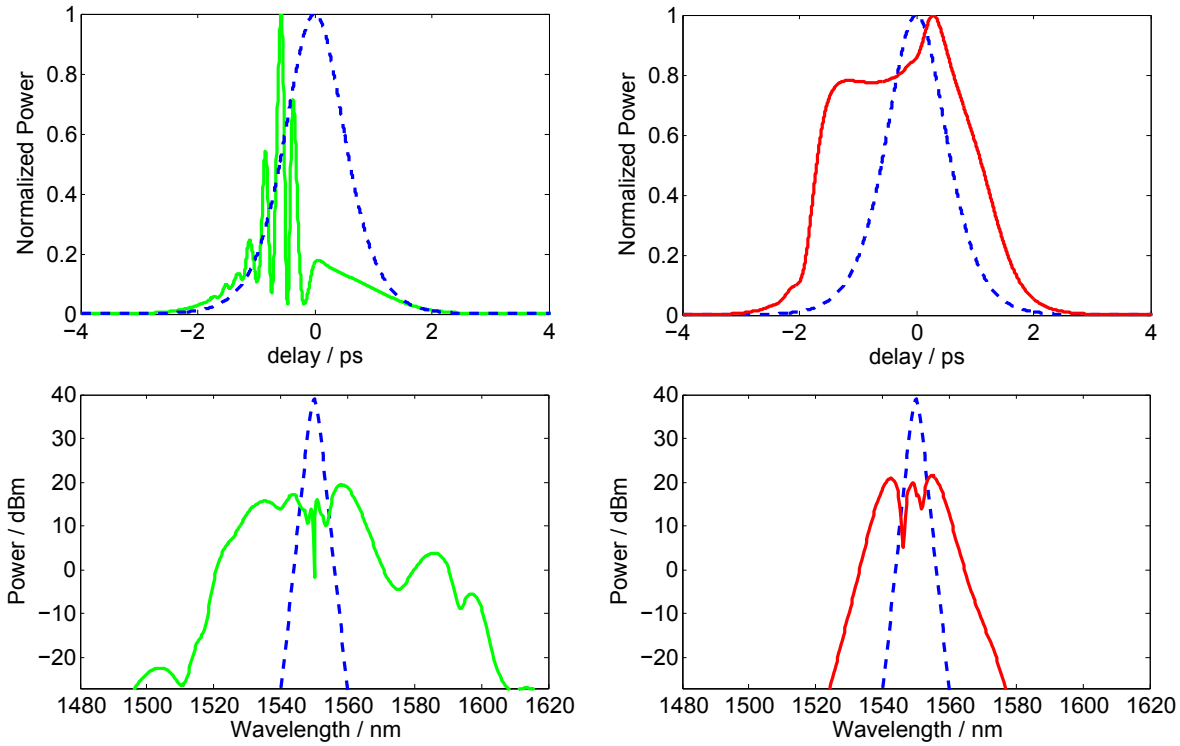

(A) Correct sign of β_2 used

(B) β_2's sign is reversed

Figure 4.3: Strong pulse propagation in a $450 \times 220nm^2$, $1cm$ long silicon photonic wire. All the effects are included. We propagate a pulse with $T_0 = 1.2\ fs$, $P_0 = 10W$. In (A), we use the correct value of GVB $\beta_2 = -3.99ps^2/m$. Green is the output temporal profile and spectrum, while dash-blue shows the input. In (B), we reverse the sign of the GVD parameter and keep everything the same. Red is used for the new output.

propagation with no change in time or spectral profile. GVD and SPM can also combine to yield a periodic evolution of the input pulse along the propagation direction. In the first case, we refer to the pulse as a a fundamental soliton while the latter is a higher-order soliton.

While solitons have been extensively investigated in optical fibres, the very nature of Si photonic wires makes it difficult for them to support solitons, at least not on very long distances. This is simply because TPA and linear losses are always acting to reduce the available peak power, and free carriers effects further complicate the picture. Nevertheless, pulses with solitonic behavior have been experimentally observed in some $5mm$

of SPW, in the TM mode(see [26]).

The present work does not investigate solitons, but rather is interested in how such features lead to greater spectral broadening. In microstructured fibers, higher-order soliton fission, accompanied with dispersive wave generation has been identified as the lead cause of broadening and continuum formation. The numerical results of Figure 3.1 suggest that the same dynamics could lead to continuum generation in SPWs, though the extent of the broadening would be severely reduced by two-photon absorption.

We illustrate the effect by choosing our own $500 \times 220nm^2$, it has a GVD coefficient of $\beta_2 = 2.95719ps^2/m$ and an effective nonlinear coefficient roughly $\sim 434.71W^{-1}.m^{-1}$. Therefore, for a $200fs$ pulse with $P_0 = 7.5W$, we obtain the soliton number $N = 3.72$, meaning that such a pulse corresponds to a third-order soliton. We increase the input peak power to $8.8W$ to compensate for the losses that occur in the first millimeters of propagation.

The results are shown in Figure 4.4. After initial SPM and pulse compression in the time domain, the original pulse breaks down into three fundamental solitons at $z \sim 1.5mm$. This corresponds to the point where the input pulse has reached its maximum bandwidth, in agreement with what is observed in fibers [20]. This distance is approximated by: $z \sim \frac{L_D}{N}$, which is roughly $1.2mm$, in agreement with what is readily seen on the plot. These fundamental solitons have different group velocities and would normally keep their shape and spectrum, but as can be seen on the density plots, further propagation is affected by linear and nonlinear losses as well as free carrier effects, and the result is the solitons losing amplitude and see their spectrum shrink along the way. We stress out once again that the TOD coefficient used here is not accurate. For larger values of TOD, the soliton fission process plays out quite differently.

What is of interest is something we briefly referred to in the previous chapter. If the input pulse is close enough to the ZDW, it would be able to transfer some of its energy in the normal regime to generate what is referred to as dispersive wave or "Cherenkov radiation." In the time domain, it manifest itself as ultrafast oscillations at the back (or front) of the output pulse. This can be seen in Figure 3.1. We use our own parameters to show this effect is possible, with what we have readily available in our lab in terms of equipment. We propagate $100fs$ pulses with peak power $P_0 = 3.7W$ in $1cm$ length of the $750 \times 220nm^2$ waveguide. This waveguide has its ZDW very close to the pump, and thus a very small $\beta_2 = -0.1568ps^2/m$ at $1.55\mu m$, which makes it our best choice for this simulation. With these parameters, the results can be seen on the figure below, showing how the dispersive wave generation significantly enhances the broadening and leads to a very broad continuum.

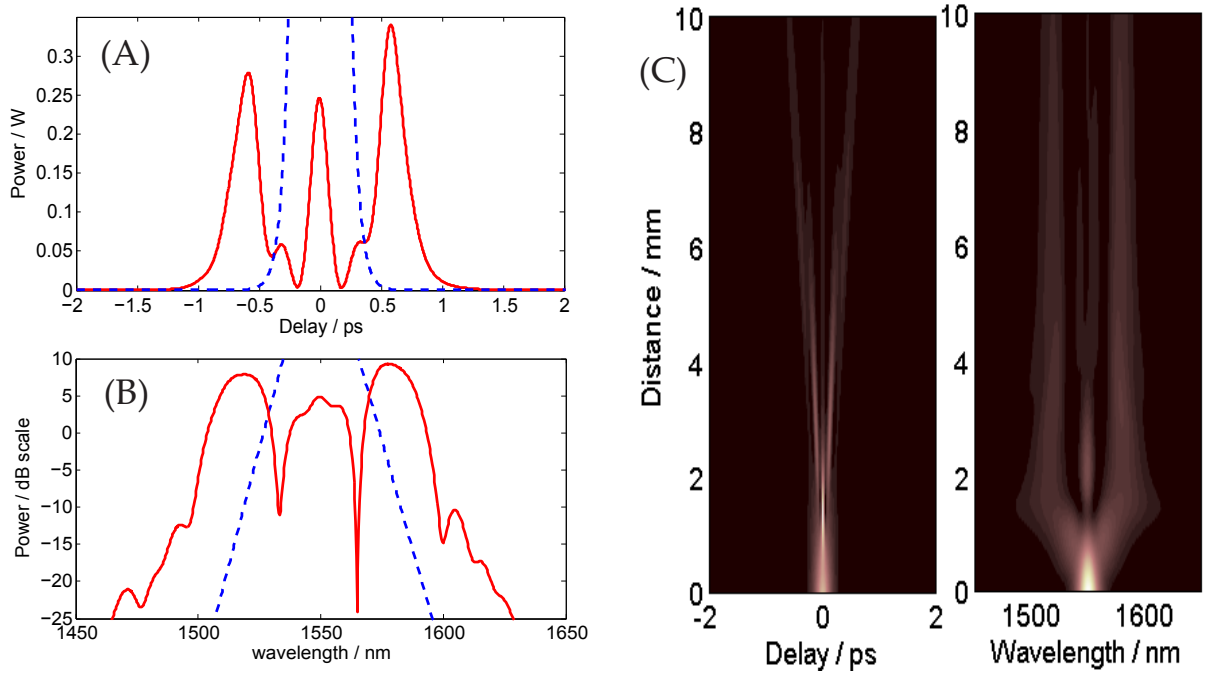

Figure 4.4: Soliton fission in a silicon photonic wire. Wire dimensions are $500 \times 220nm^2$, propagation length $1cm$ and the input pulse parameters $P_0 = 8.8W$, $T_0 = 200fs$. (A)Time domain input(blue) and output(red). (B) Input(blue) and output(red) spectra. (C) Time domain and spectral density evolution along the waveguide length.

The frequency of the dispersive wave can be found from [28]:

$$\frac{\omega_d}{2\pi} = -3\frac{\beta_2}{\beta_3} + \frac{Re(\gamma)P_s\beta_3}{3\beta_2^2} \tag{4.2}$$

where P_s is the power of the soliton that is perturbed. taking $P_s = P_0 = 3.7W$, we find that the dispersive wave frequency corresponds to a wavelength of $\lambda_d \simeq 1.36\mu m$, which agrees well with our simulation results of Figure 4.5.

Soliton dynamics have been used to explain continuum as broad as $350nm$ in SPW (see Hsieh et al. [29]), and indeed, the results of those experiments have a good qualitative agreement with our plots of Figure 4.5.

We close this section by remarking that, though we have discussed soliton dynamics using only femtosecond pulses, such effects can be seen also when longer pulses are

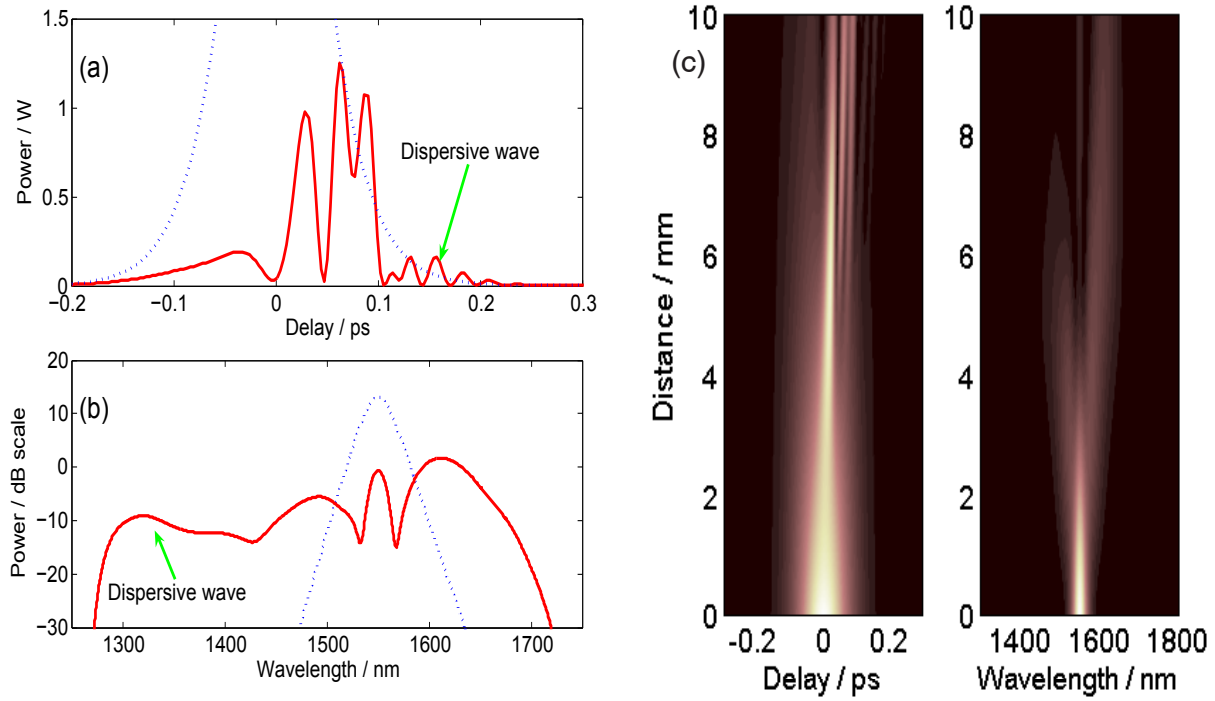

Figure 4.5: Soliton fission and dispersive wave generation in a $750 \times 220nm^2$, propagation length $1cm$ and the input pulse parameters $P_0 = 3.7W$, $T_0 = 100fs$. (a)shows our results in the time domain, the blue line being the input. (b)plots the input and output spectra (c) Density plots on the linear scale.

used. As evidence, when we increased the peak power of a picosecond pulse to $10W$, the pulse broke down into a train of much shorter pulses(Figure 4.3). Each of those pulses can behave as a soliton and thus undergo all the dynamics described in this section and undergo dispersive wave generation, at least in theory. Continua attributed to soliton dynamics have been generated in fibers with nanosecond probing pulses, by careful design of fibre parameters.

4.4 Four-wave mixing and Modulation Instability

Another class of processes that will influence spectral broadening and continuum generation are parametric processes. We will limit ourselves to four-wave mixing (FWM) and give only a brief description of it. As the name indicates, FWM refers to the frequency mixing that occur when photons of different frequencies are present in the waveguide. The figure below shows a simple illustration of the process. ω_1 and ω_3 are two pump waves, ω_s is the signal wave and ω_2 is referred to as an idler. The interesting case is when the two pump waves have the same frequency. What then occurs is the conversion of the pump into two side bands that are downshifted and upshifted. The efficiency however depends on phase-matching conditions, that is why it is a parametric process. In supercontinuum generation, FWM can play a role provided that the pump is close enough to the GVD so that phase matching can be achieved. It is usually predominant in the case of picosecond or longer pulses (see Dudley et al . [19]).

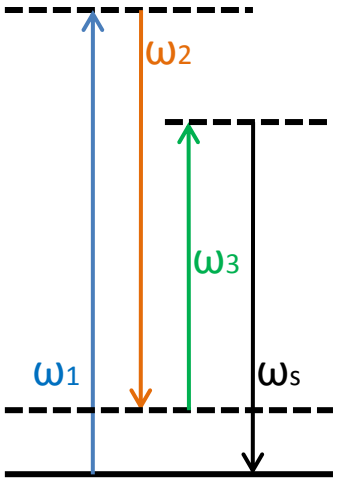

Figure 4.6: Photon picture of Four-wave mixing

Modulation Instability corresponds to the unstable evolution of a continuous wave beam that is copropagating in the medium with either a pulse train or another CW

beam. For the degenerate case, it will be the growth from noise of two sidebands that are symmetric with respect to the pump frequency. It is therefore obvious that MI and four-wave mixing are two different descriptions of the same fundamental process, one in the time domain (MI) and the other in the frequency domain (FWM).

Both phenomena have been demonstrated in Si photonic wires [30, 31] and can be properly modeled by using coupled propagation equations and the correct nonlinear polarizations. As we did not consider this in detail, we include the phenomenon here for completeness.

4.5 Limiting nature of continuum generation in Si photonic wires

We have now outlined the most important mechanisms that would lead to spectral broadening in SPWs. The logical question to ask then is, how broad can we make such a continuum? Are there some features of it we can engineer?

One would normally expect that when pumping with short pulses with the same width, spectral broadening would increase with peak power. However, this does not always hold for SPWs. We have already seen the impact of two-photon absorption in reducing the spectral broadening in SPM for example, and this is rather intuitive. We also showed how free carrier dispersion interacts with the kerr effect to produce a net blue shift in ps pulses SPM spectra. The cumulation of these processes, but mainly TPA, impose a limit on how broad a continuum generated in Si wires can be.

To see this, we model the propagation inside a centimeter long $750 \times 220nm^2$ wire of $212fs$ pulses with different peak powers. The recorded spectra are shown in the waterfall plot of Figure 4.7. From the bandwidth versus peak power plot, we see that after almost linear growth, the bandwidth comes to some sort of "saturation" and thereafter, it increases only modestly.

We calculated the bandwidth plot by subtracting the shorter wavelength for which the amplitude is $-30dB$ from the longer one. While this does not tell us about the spectral features of the generated continua, it tells us enough about the nature of the limit in broadening. This limiting effect has been observed both numericall and in experiments by a number of researchers in the field(see [8, 29, 7]). Thus, for a given pulsewidth, shape and waveguide parameters, there is a limit in how broad the generated continuum will be. As can be seen from the figure, the spectral content of the continua actually change very little, and this implies that we will see the same limiting effect in terms of

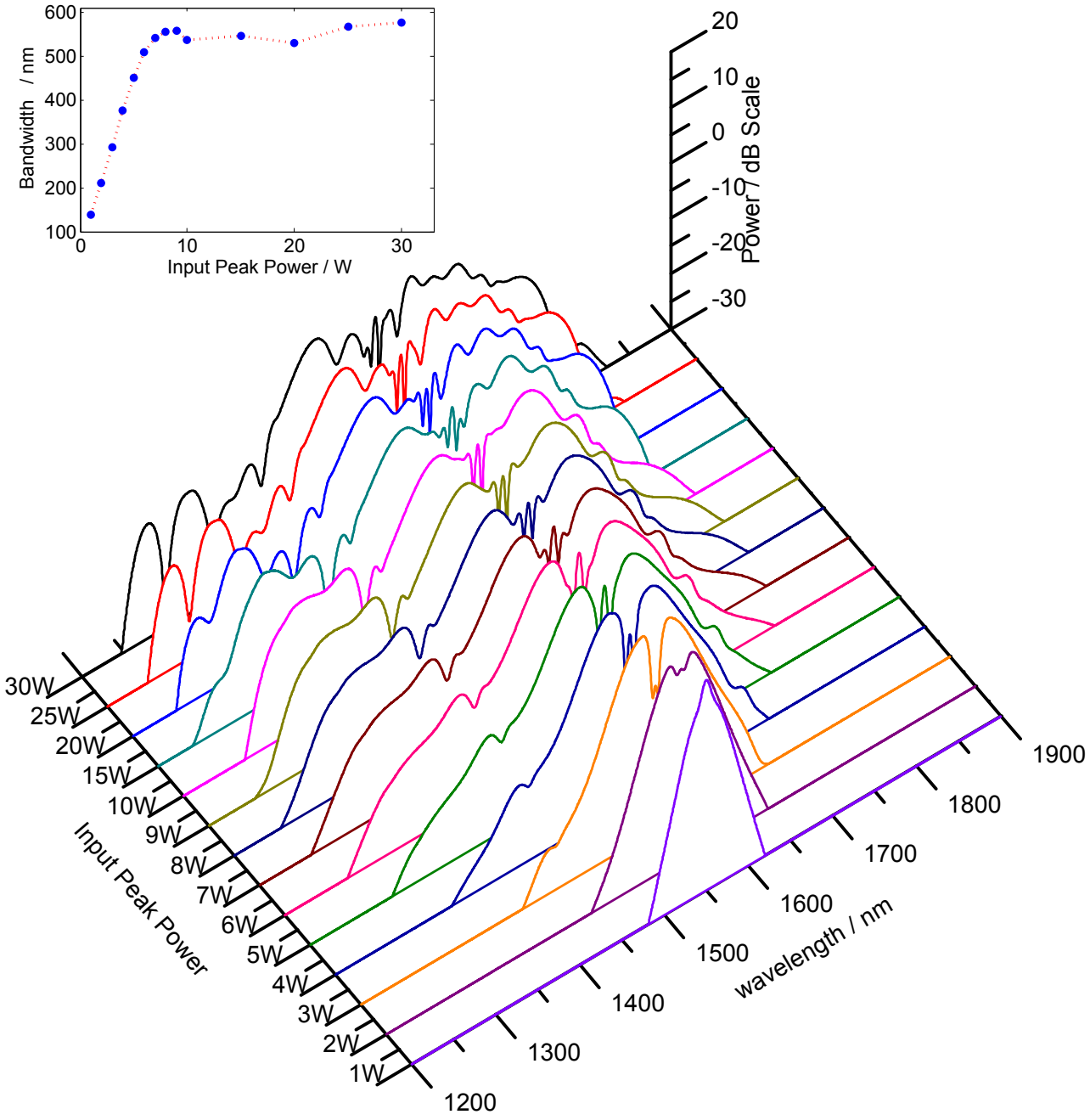

Figure 4.7: Limiting nature of continuum generation in SPW. $212fs$ pulses are propagated in a centimeter long, $750 \times 220nm^2$ waveguide. The simulated spectra show a "saturation" in bandwidth. This limiting phenomenon is inherent to the Nature of Si photonic wires and is largely due to TPA.

power transmission of the waveguide when peak power is enough to induce broadening. This has been termed "optical limiting". What we mean by that is, a plot of average output power versus input peak power for this femtosecond pumping, would show the same saturation effect. Though we only showed our results here using femtosecond pulses, the same limiting behavior occurs for picosecond or longer pulses.

On a side note, it is instructing to look at the plots of Figure 4.7. For peak powers from 3 to 10W, the output spectrum shows the very same features. We see a distinct peak start to appear near 1400nm and remains at that wavelength for several input peak powers, this is evidence to soliton formation inside the waveguide. The energy carried by this soliton increases with input peak power and when high enough, this soliton itself is perturbed by propagation. This explain the changes in spectral features for very high input peak powers(20 to 30W). It is by tracking this soliton formation process in experiments that Hsieh et al. [25] extracted the correct value for the TOD coefficient.

4.6 Summary

We have covered here the nonlinear processes that stem from the interaction between dispersive effects and third-order nonlinearities, as well as free carriers effects in SPWs. We have shown the possibility of continuum generation, and also saw that such continua will be inherently limited by two-photon absorption. As all the modeling were done with parameters available to us in the lab, we now turn into the experimental investigation of nonlinear effects in SPWs.

Chapter 5

Experimental investigation of nonlinear processes in Si photonic Wires

In this chapter, we present our own experimental investigations of the nonlinear phenomena we have described so far. We describe the problems that were encountered in so doing, and our attempts to solve them. We draw whenever possible, a comparison between numerical and experimental results. We stress out once again that, our aim was to investigate the possibility of continuum generation in Si wires, and the discussion herein is limited to the output spectra recorded in our experiments.

5.1 Picosecond pulse propagation in Si photonic wires

5.1.1 Experimental setup

The first part of our work consists of experiments with a picosecond laser source. The laser source uses an electro-optic modulator to achieve modelocking and delivers pulses from 1.5 to 11ps. The setup for the experiments is shown below.

The electro-modulator is operated by a radio-frequency signal at $\sim 10GHz$, and thus the laser's output has this repetition rate. The problem with such a high repetition rate is twofold. First of all the peak power available to each pulse is substantially lower, even when amplified. Most importantly, however, the pulse separation in time is only $\sim 100ps$. This is far shorter than the average carrier lifetime in Si wires, which despite the fact that carriers can quickly diffuse to the surfaces and recombine, is still of the order of 1ns. The result is that it would be impossible for us to observe any nonlinear effects over a broad range of input powers, and we attribute that to the fact that free

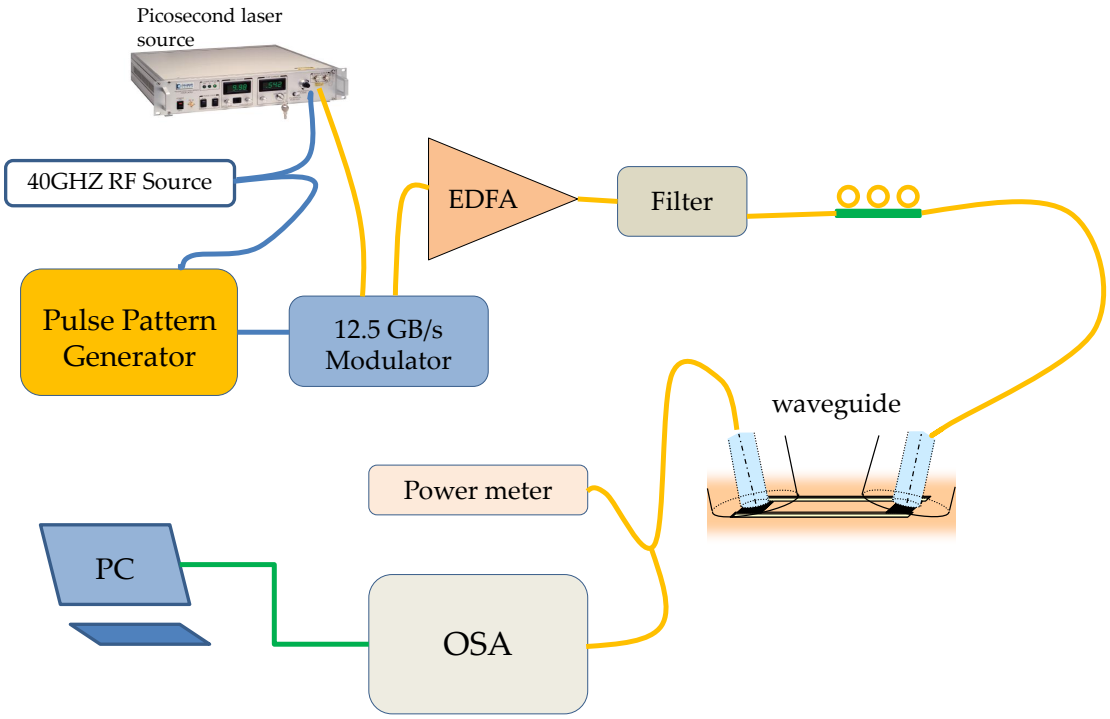

Figure 5.1: Setup for experiments with picosecond pulses. Yellow connectors represent optical fibres used to transport the light signal, and the blue ones are RF connections. The OSA is connected to the PC with a GPIB cable and data is captured using LabView.

carriers would be able to accumulate from pulse to pulse and thus enhance the FCA, significantly reducing the power available to excite nonlinearities (see [23]).

The way around was to use a pulse pattern generator and a modulator in a configuration that would act as a pulse picker. There are imperfections in this setup as the modulation process loses us some 10 to 15dB of average power, and the pulses on either side of the one that is selected cannot be entirely suppressed. This then creates the need to put an amplifier after the modulator and then a filter to get rid of the ASE noise. Finally, a polarization controlling wheel is inserted so that we optimize the coupling of the TE mode through the grating we described in Chapter 1. At the output, we measure the average power and record the spectrum.

5.1.2 Self-phase modulation using picosecond pulses

We investigated SPM in the different wire waveguides available to us. With modulation settings carefully adjusted, we were able to record spectra that showed the trademark of self-phase modulation.

SPM in the $5mm$, $450 \times 220nm^2$ waveguide

It took some time to reach the proper configuration and choose the settings that would allow us to see some of the nonlinear effects we expect with picosecond pulses. One we already referred to is the high repetition rate of the source. Though our "pulse picker" can be adjusted at will at allow us to pick only one pulse in a few thousands, it is important to keep in mind that the pulses are amplified afterward. If the modulation rate is too high, the pulse train emerging from the modulator has very low average power and the amplification process will not be ideal (EDFA has optimum performance when input power is $0dBm$, at the modulator output, average power is usually -20 to $-10dBm$).

Figure 5.2 shows the SPM spectra we recorded for a $5mm$ long waveguide. We chose both 48 and 96 bits modulation sequence, in each case, the estimated peak power is roughly $P_0 \sim 1.6W$. The figure also shows the recorded output spectrum when no modulation is applied on the signal and it keeps its original repetition rate. The estimated peak power for that case is $P_0 \sim 1.2W$ and as we can see, no broadening whatsoever does occur.

The figure also shows our simulation with the parameters we estimated, and as can be seen, there is quite a good qualitative agreement. Experimental spectra are more shifted to the left than it actually should, and the peak-like feature in the simulation seems to be absent. Nevertheless, the agreement between the two is quite good.

SPM in the $10mm$, $650 \times 220nm^2$ waveguide

We used a waveguide twice as long as previous one and slightly wider, and recorded similar spectra, the broadening of which we once gain attribute to SPM. Figure 5.3 below shows the recorded spectra and corresponding simulations. There is once again a very good qualtative agreement between simulation and experiment here. However, the experimental spectra are more shifted to the blue and for $P0 = 6.3W$ (green curves), the phase change in experiments does not correspond to what we have from simulations. Two things could be possibly responsible for the discrepancies, a chirp applied

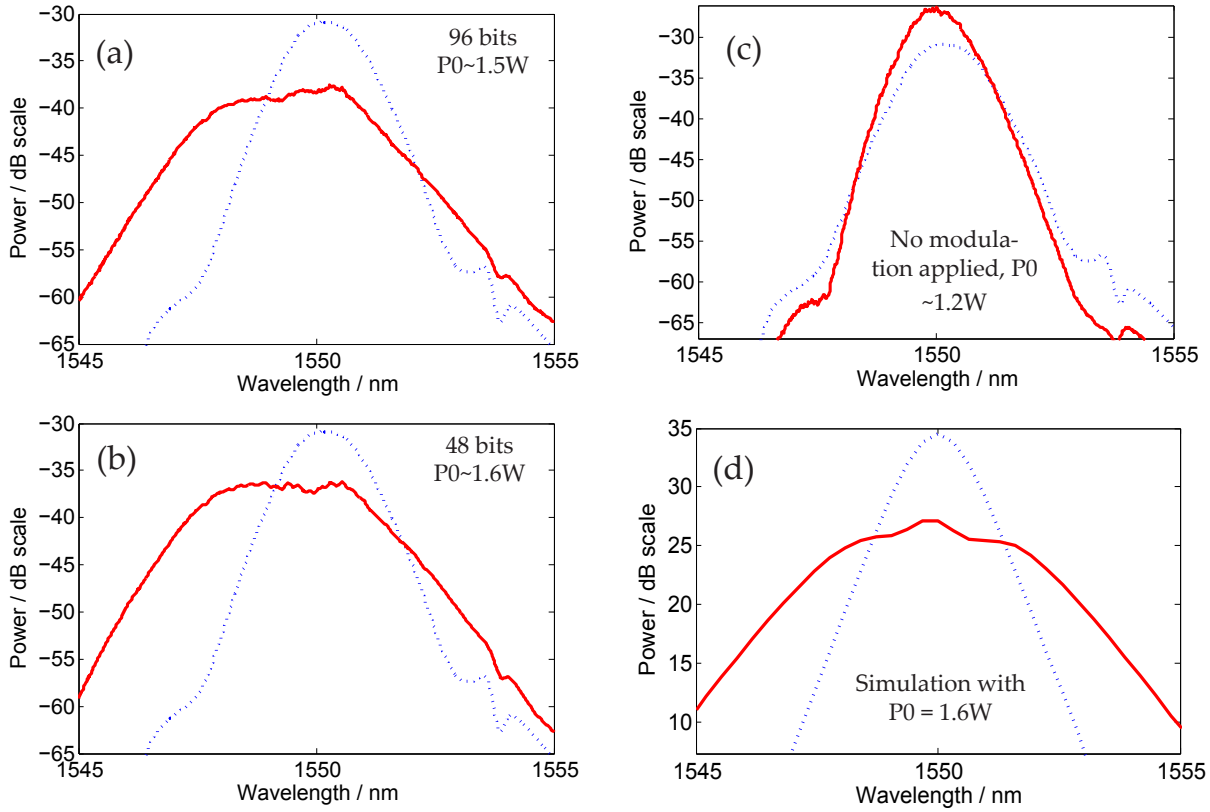

Figure 5.2: Self-phase modulation of $1.8ps$ pulses propagating inside a $450 \times 220nm^2$, $5mm$ long Si photonic wire. (a) 96 bits of modulation, and thus Repetition rate of $103.68MHz$, input average power is $5mW$ at the EDFA and estimated peak power at the input of waveguide is $1.5W$. (b) Repetition rate is doubled and so is the average power to keep up with roughly the same peak power. (c) No modulation applied on the pulses. (d) Corresponding simulation. In all cases, blue line is input spectrum and red is the output

on the input pulse at the input grating, or perhaps thermal effects. In fact as the chip heats up, the net result is a small change in the silicon refractive index. Both could actually result in the asymmetry and different phase change.

The fact that the pulses from the original pulse train cannot be totally suppressed at the modulator might also play a role, because once amplified, they might have significant power and thus feel the effects of the free carriers generated by the much

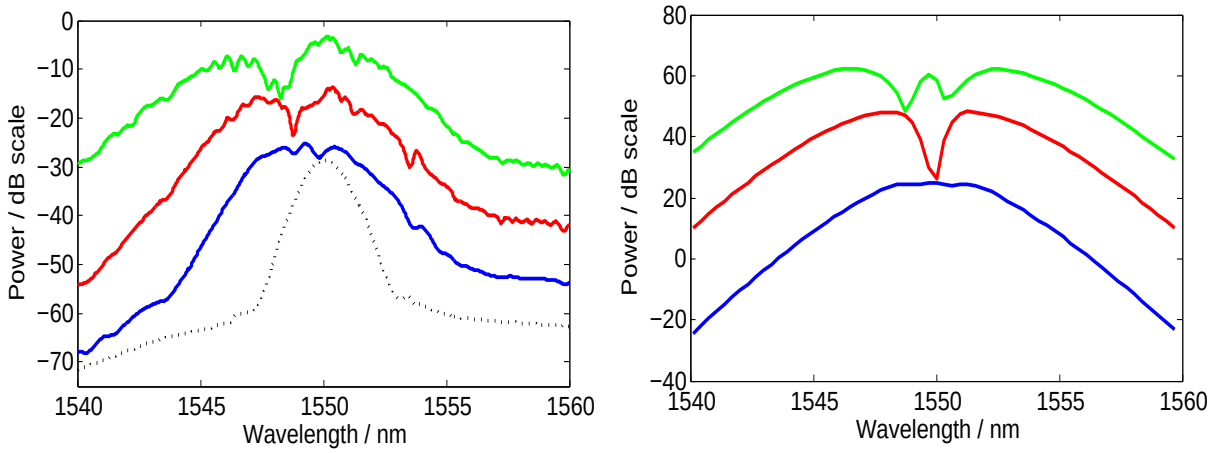

(A) Experiments (B) Simulations

Figure 5.3: Self-phase modulation of $1.8ps$ pulses propagating inside a $650 \times 220nm^2$, $1cm$ long Si photonic wire. (a) Recorded spectra with a $48bits$ modulation pattern. (b) Corresponding simulations. Dashed curve is the input spectrum recorded after the filter, while blue, red and green are spectra with estimated peak powers 1.6, 3.2 and $6.3W$ respectively.

stronger pulse. For such high peak powers though, the nonlinear loss is significant. With $I = \frac{P_0}{Aeff} \sim 6GW/cm^2$ and the TPA coefficient $\beta_T PA = 5 \times 10^{-12} m/W$, the nonlinear loss coefficient is $\alpha_{NL} = 3cm^{-1} = 13dB/cm$. This is why the peak power greatly decreases in the first few millimeters of propagation.

5.1.3 Further broadening with picosecond pulses

In the previous chapter, we explained how a strong picosecond pulse could undergo severe distortion, yield a train of far shorter pulses while also producing significant broadening. Here we attempted to verify those concepts experimentally and pumped our waveguide with $1.8ps$ pulses of increasing peak powers. Our results are shown in the waterfall plot below.

It is obvious that, after $1cm$ of propagation, the original spectrum is very much distorted, and its shape as well as bandwidh depend very much on the input peak power when it is kept low enough. As the peak power increases, the nonlinear loss becomes more and more important, and there is little change in the resulting spectra. The dis-

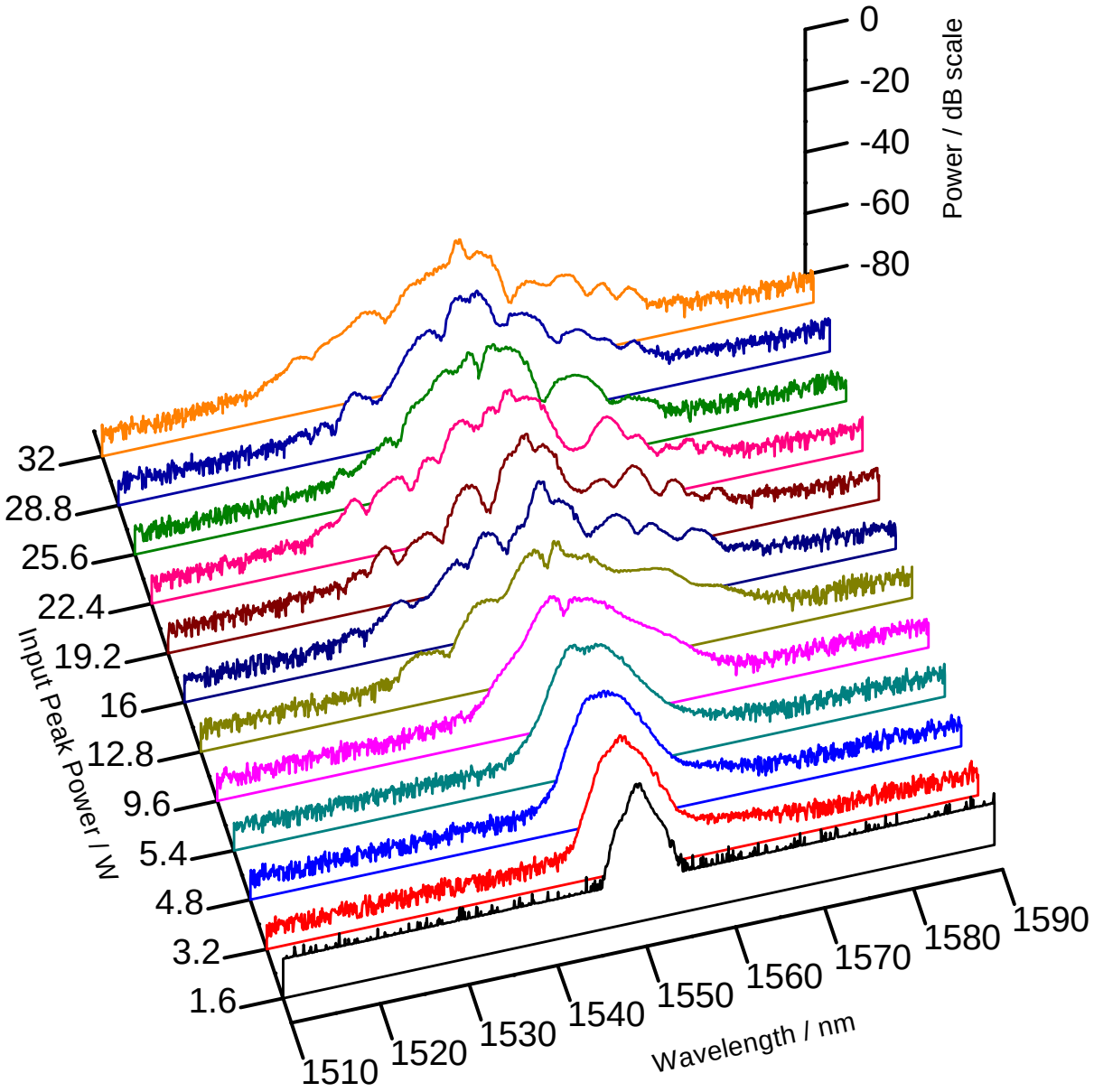

Figure 5.4: Picosecond pulse broadening in $450 \times 220nm^2$, $1cm$ long Si photonic wire as a function of increasing peak powers.

parity between the experimental results and our simulations are however, more pronounced. To see this, we have sampled out the example of $P_0 = 25.6W$ and plot it below along with our numerical results. For this value of peak power, the nonlinear loss increases to $\alpha_{NL} = 54.2dB/cm$, and the pulse is very much attenuated in the first

millimeters of propagation. The net result is the limiting process we referred to earlier.

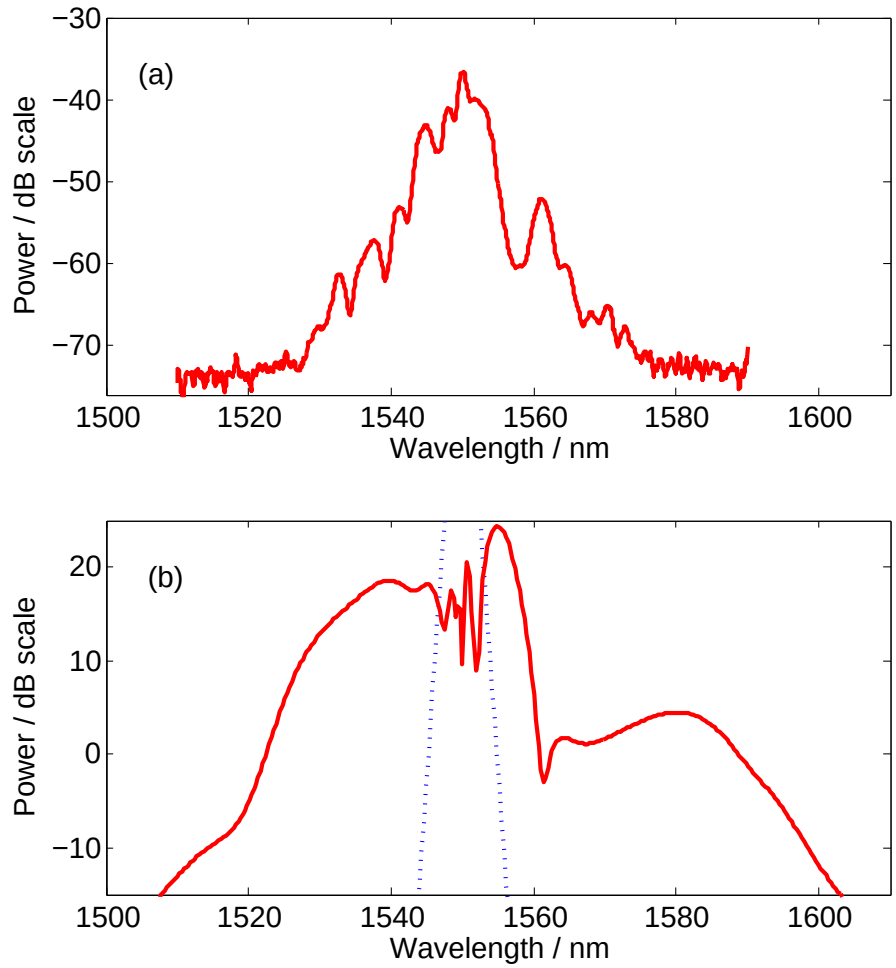

Figure 5.5: Broadening of a $1.8ps$ pulse with $P_0 = 22.4W$ in a $450 \times 220nm^2$, $1cm$ long Si photonic wire. (a) Experimental measurement, (b) Modeling

Though some comparison can be drawn between our experimental results and what we obtained from modeling, the resemblance is very little. We believe a number of factors might be responsible for the discrepancies. Our input pulses are not exactly $sech^2$ pulses, and the fact that they are modulated, amplified and filtered make the correct estimate of pulse shape and power rather difficult. Second, for these experiments, we used gratings to couple both in and out of the waveguide, gratings have a limited bandwidth of roughly $30nm$ over which they are efficient, and it is possible that they impinge

an additional chirp, albeit very small, on the pulses.

Nevertheless, qualitative features can still be discussed as regarding Figures 5.4 and 5.5. For peak powers from 16 to 25.6W, there is a distinct feature next to the central peak, around 1560 $\sim$ 1570nm. This peak also appears in simulations, although broader, and we attribute it to a soliton that starts to form as the peak power is increased.

5.1.4 Optical Limiting with picosecond pulses

As discussed at the end of the previous chapter, and also evident from Figure 5.4, spectral broadening in Si wires will experience some sort of "saturation". The consequence of this is that there will be a similar limiting effect in terms of power transmission of the wire.

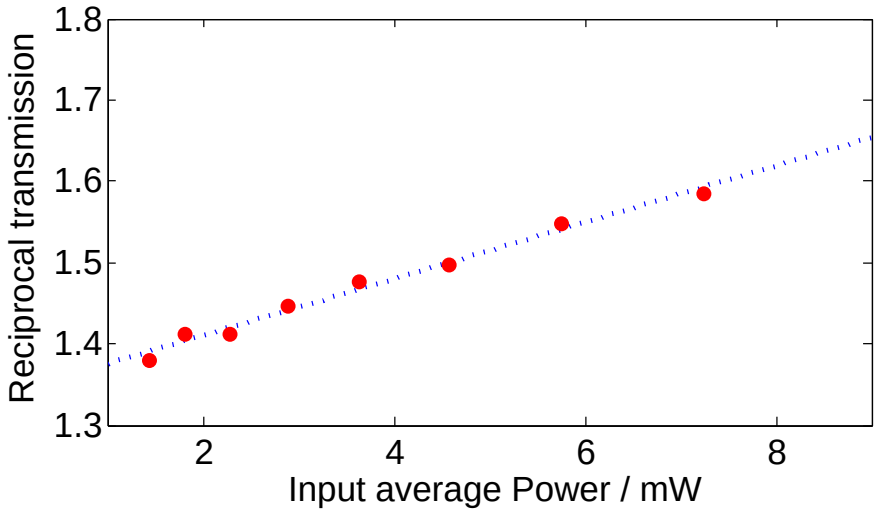

Figure 5.6: Optical limiting in a 5mm -long, 450 $\times$ 220nm^2 Si photonic wire. The input is a train of 1.8ps pulses with 207.36MHz repetition rate. Plotted on the figure is the reciprocal transmission $\frac{1}{T} = \frac{P_{in}}{P_{out}}$ of the waveguide as a function of input average power.

Figure 5.6 shows a plot of experimental transmission data for a 5mm long, 450 $\times$ 220nm^2 wire. Instead of a flat horizontal line as would be the case for a perfectly linear device, the curve of $\frac{1}{T}$ is instead a straight line with a positive slope. This is a clear indication, that the loss experienced by a propagating pulse will increase with its peak power. Such a pulse will then suffers significant loss in the first few mm of propagation, before further propagation results in broadening. TPA is therefore responsible for the

limiting effect we observe and also justifies the limit that can be attained in spectral broadening.

5.2 Femtosecond pulse propagation in Si photonic wires

We next present our investigation of nonlinear spectral broadening in Si photonic wires. The setup for the experiments is very similar to that of Figure 5.1, and is shown below. except the picosecond laser source is replaced by another laser that uses a saturable absorber to achieve modelocking. It delivers pulses from 350 to $86fs$, at a repetition rate of $20MHz$ and with peak powers from 400 to $9.8kW$. Such high peak powers represent the problem we battled with for a long time, in that the pulse would at best undergo strong self phase modulation in the delivering fibers before reaching the waveguide, or worse, would behave as a higher-order fiber soliton. In the latter case, it appears that choosing the length of the connecting patchcord such that the higher-order soliton is just recombining as it enters the waveguide would be a good solution. This assumes however, that no other nonlinear effects in the fiber such as high-order dispersion or even Raman Scattering would disturb the soliton. To rule out fiber influence, we placed an attenuator right at the output of the source, attenuating the pulses such that they would undergo no distortion inside the fibers. In so doing however, it appeared in experiments that the peak powers were much reduced and we did not get to see some of the effects predicted in modeling. Even in this case it has been nearly impossible to give an interpretation of the data obtained, and more difficult to compare it to modeling results.

5.2.1 Source characterization

We characterize the source by measuring its spectrum, as no equipment is available to view the pulses in the time domain. As we said in the previous section, such a spectrum will once again depend on the length of the fiber between source and spectrum analyzer, and that is exactly what we observed. For the measurements in which we connected the source directly to the waveguide, we used a fiber as short as possible. We present here the recorded spectra when the connecting fiber is $30cm$ and $2m$ long.

It is clear that even with the shortest possible length of fiber, the source does not deliver $sech^2$ pulses. The spectrum depends much on the fiber length. We suppress this dependence by inserting a $15dB$ attenuator right at the output of the laser source, but of

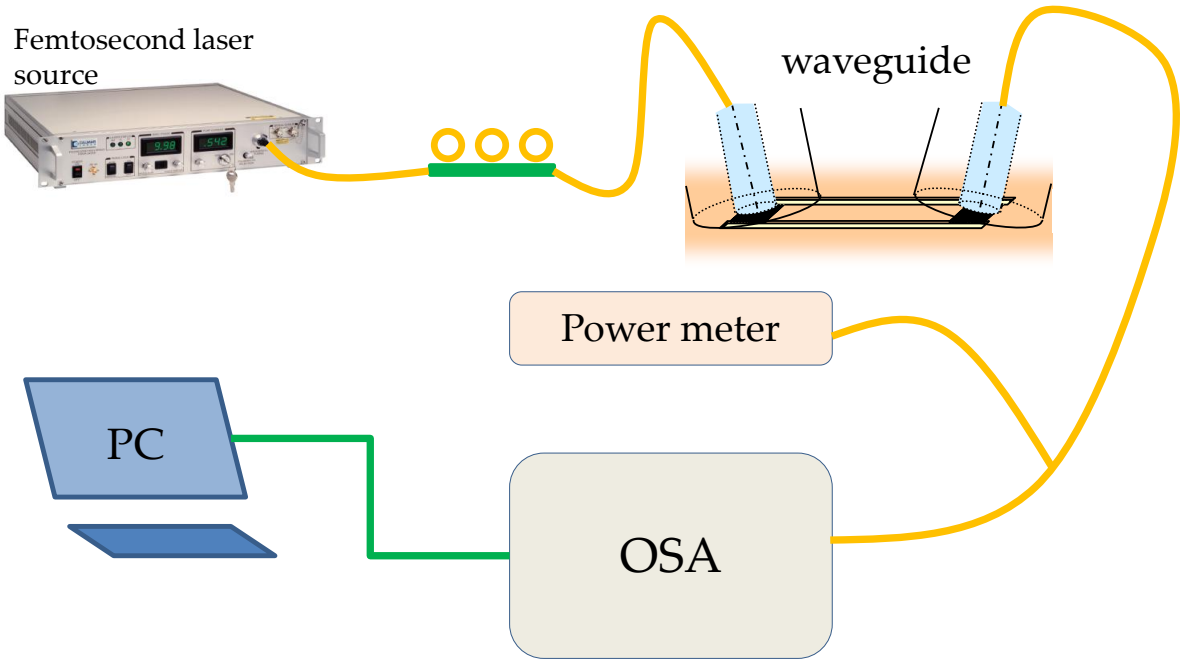

Figure 5.7: Setup for experiments with femtosecond pulses.

course, it takes away some of the peak power available to us.

5.2.2 Results with non-attenuated pulses

Before we acquired an attenuating device to reduce the pulse peak power and rule out fiber influence, we conducted some experiments in which the pulses were delivered to the waveguide with the shortest possible length of fiber. Though we cannot compare the results of such experiments to our numerical modeling, the effect of the Si wire waveguides on the pulses can be extracted when comparing to the input.

a) The $350 \times 220nm^2$ waveguide, vertical in and out-coupling

Figure 5.9 shows the recorded spectra with the estimated values of pulsewidth and peak powers. These two cannot be separately adjusted for our source, unfortunately. The values with question marks are estimated from manufacturer data, and the peak powers are computed with the coupling loss values obtained from our measurements. On very short reference waveguides and with very low input power, the fiber-to-fiber

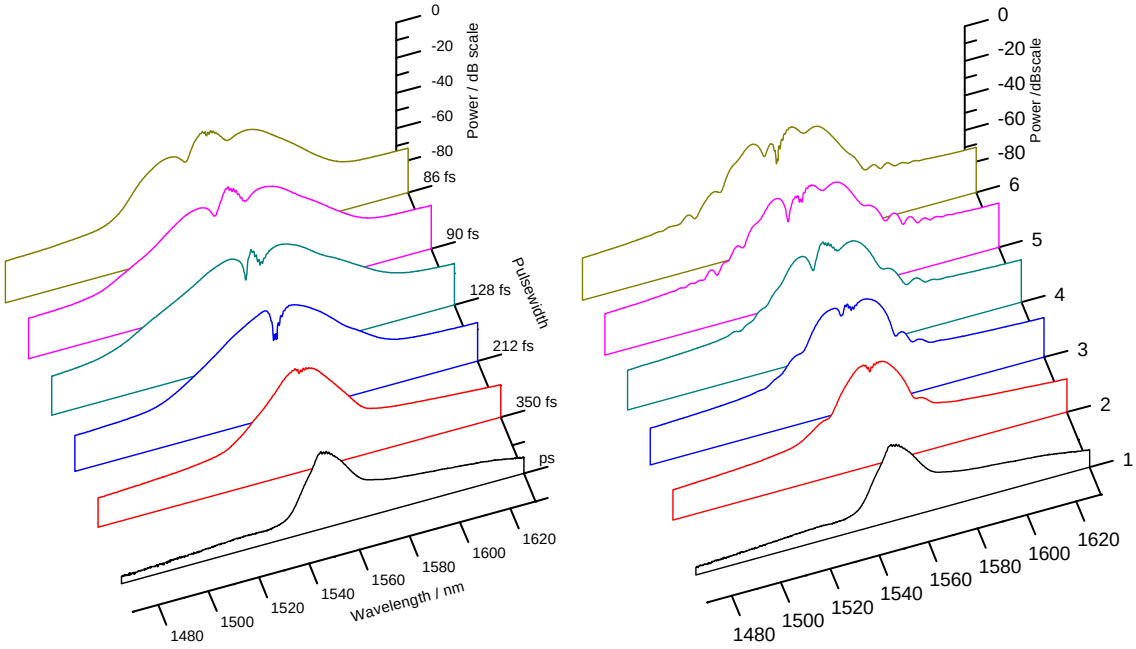

(A) Fiber length $= 30cm$ (B) Fiber length $= 2m$

Figure 5.8: Impact of patchcord length on the spectrum of the femtosecond source when no attenuator is inserted at the output of our laser source.

loss value is $14.6dB$, half of which we attribute to the input grating and thus obtain the peak powers above. Comparing with Figure 5.10(A), we see that the spectrum is altered and broadened in the Si photonic wire and part of the energy is transferred into the anomalous GVD regime. However, for such high peak powers, the broadening we expect from such a wire is very different.

b) The $450 \times 220nm^2$ waveguide

We carried out the same measurements with this centimeter-long $450 \times 220nm^2$ waveguide and the results are shown in Figure 5.10. In part (A), we use the same setup as previously and the connector length is quite short, around $50cm$. Light is coupled in and out vertically using the gratings. In (B), the connector length is much longer, about $2m$, and light is out-coupled horizontally as we have removed the output coupler. The sharp differences between the two figures stress out the effect of the connecting patchcords and make it very difficult for us to interpret the data and find out which mechanisms

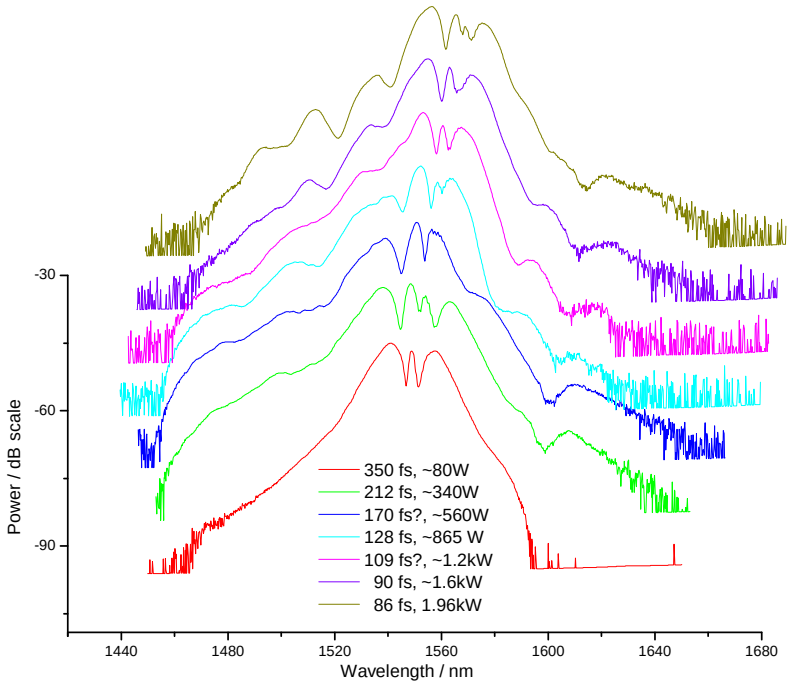

Figure 5.9: Recorded spectra with the femtosecond source as input. Pulses are propagated in a centimeter-long $350 \times 220nm^2$ wire.

leading to broadening are actually going on in the Si wire.

Simulations with such short pulsewidths and high peak power show the soliton dynamics we discussed in the previous chapter. In our experiments however, we fail to observe any such effects. We suspect that the pulses entering the Si wire are distorted and very different from what we might assume they are, since simulations with $sech^2$ pulses or second order solitons yield very different results.

c) The $750 \times 220nm^2$ waveguide

Similar spectra are recorded for this much wider waveguide, as shown in the plots of Figure 5.11 below. The distortion impinged upon the pulses is evident from the plots showing the $20dB$ bandwidth of the output spectra, which is as broad as $100nm$ for the $90fs$ pulses. Still, it is very difficult to speculate on the nature of the broadening, though we suspect SPM plays a role. The effects of GVD can also be indirectly deduced by comparing the spectra obtained for different waveguides. For the $350 \times 220nm$ waveguide for example, the pulses are propagating in the normal GVD regime, and mostly SPM

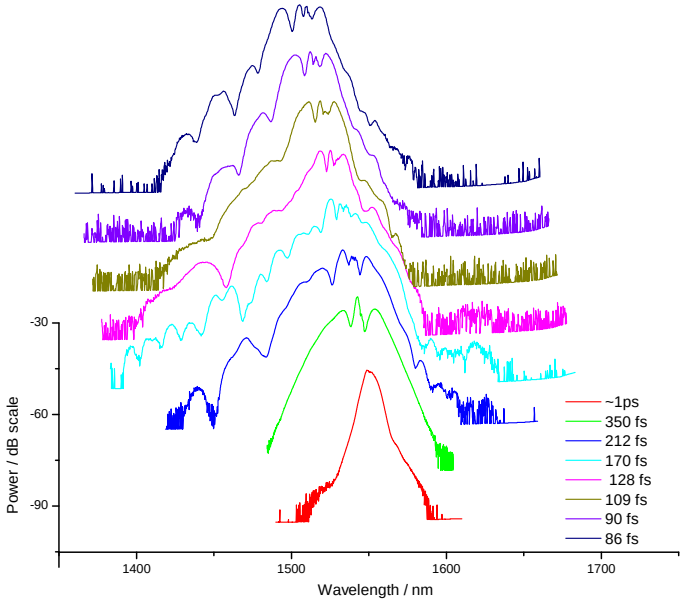

(A) Vertical in and out-coupling, with a connector length of roughly 50cm between source and waveguide

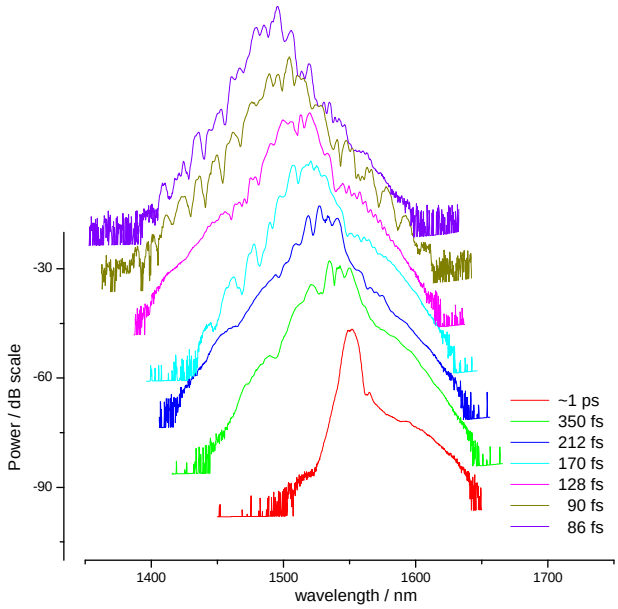

(B) Vertical in and horizontal out-coupling, connector length roughly 2m

Figure 5.10: Recorded spectra for pulses propagating inside a centimeter long $350 \times 220nm^2$ Si wire.

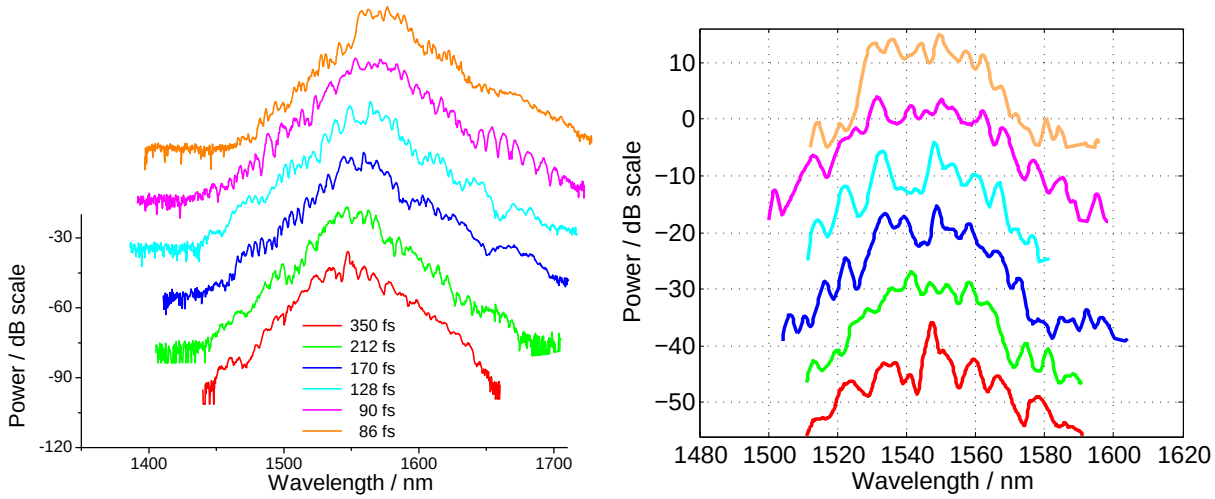

(A) (B)

Figure 5.11: Pulses are propagated in a centimeter-long $750 \times 220nm^2$ wire and output coupling is done horizontally with a lensed-fibre. (A)Recorded spectra, (B) $20dB$ bandwidth of the spectra, for clarity, we add a $10dB$ offset for each plot.

affects their propagation with some transfer of energy in the anomalous regime. For this wider waveguide, while we are close to the ZDW, we are pumping in the anomalous regime and most of the broadening does occur there, though some energy also is transferred in the blue.

5.2.3 Measurements with attenuated pulses

We acquired attenuating devices which would take down the pulse peak powers so that no nonlinear effect in the delivering fiber would influence their shape. In so doing, the attenuating device was to overcome the disadvantage of the tunable attenuators available, in that no fiber would be inserted between the source and itself. This was done under the assumption that the resulting peak powers would still be enough to allow us to observe the nonlinear effects in Si wires.

To make sure the attenuator actually reduces the power to the extent the delivering fibers don't affect it, we recorded the spectra using 0.75 and $2m$ long fibers. As can be seen from Figure 5.12, the length of the fiber no longer influences the recorded spectrum.

It can still be seen however, that the shape of the spectrum is not the typical $sech^2$ or

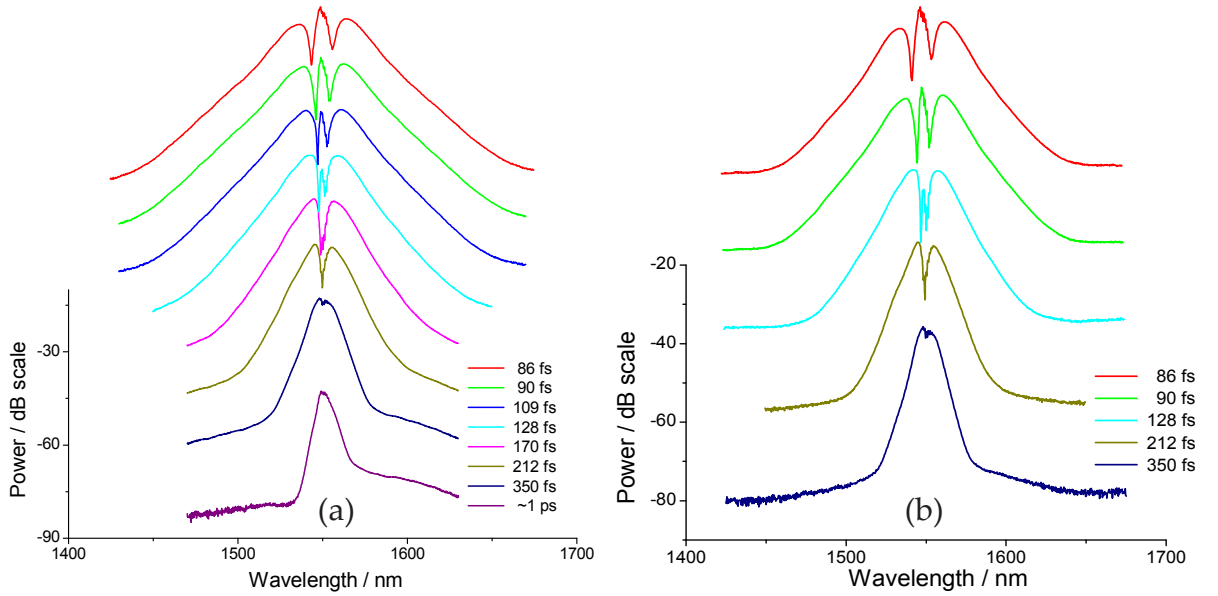

Figure 5.12: Recorded spectra of our femtosecond source when a $15dB$ attenuator is attached at its output. (a) A $75cm$ patchcord guides the pulses to the optical spectrum analyzer. (b) A much longer fiber, $2m$, is used.

gaussian shape we typically use in modeling. Rather, we also see the peaks that develop as the amplifying current for the laser source is increased and the pulse shortened. The spectra however are in conformity with the data from the manufacturer.

Next, we carried out measurements using the attenuated pulses. Surprisingly, the waveguides we measured on, that is $450, 550, 650$ and $\times 220nm^2$ showed a somewhat similar response, making a full comprehension of the phenomena even more difficult. Below, on Figure 5.13 are for example the recorded spectra after $1cm$ of propagation inside the $w = 750nm$ and $w = 550nm$. The distortion resulting from the propagation inside the wires is clear, but as they do not correspond to any of the effects that can be tracked in modeling, it is difficult to attribute it to any particular nonlinear process, especially since the response from the two waveguides is similar. For the pulse parameters $350fs$ and $P_0 = 2.53W$, assuming a sech pulse, the $550 \times 220nm^2$ waveguide would affect the pulse by breaking it into three solitons, though not resulting in huge broadening. As for the $750 \times 220nm^2$, the pulses would only undergo self-phase modulation according to our modeling, which are shown on Figure 5.14. Experiments however, show the original spectrum partitioned into somewhat symmetric halves around the

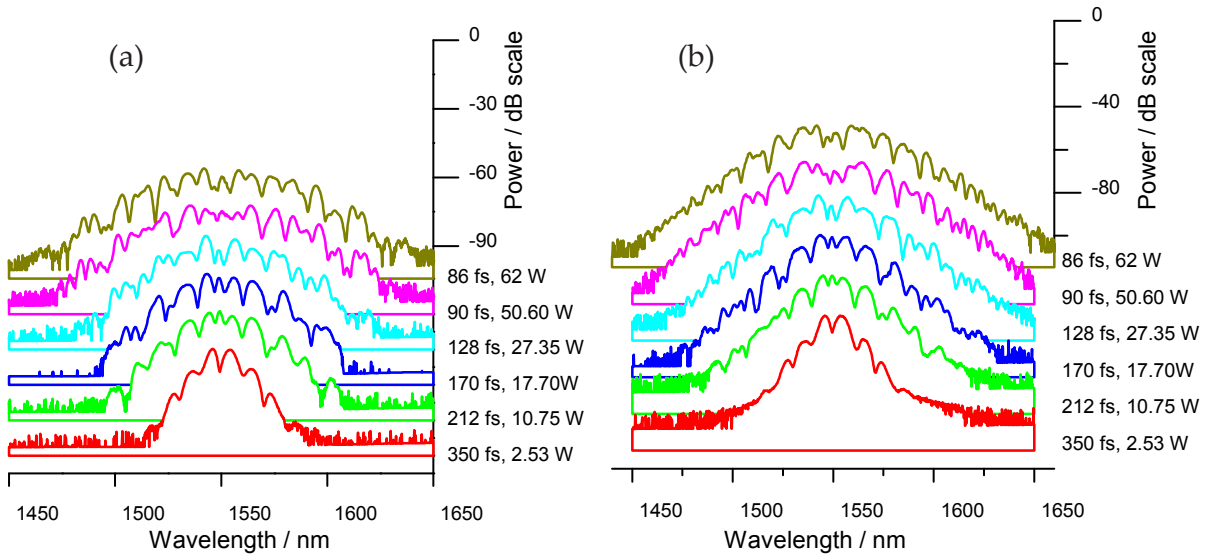

Figure 5.13: Spectra recorded at the output of the wire waveguides with the original pulses attenuated by $15dB$, and the input spectra shown in Figure 5.12. The peak powers are calculated by assuming a loss of $7dB$ at the input grating, which is moderate as the new gratings have higher efficiencies. Light is coupled out horizontally from a cleaved facet. (a) $w = 550nm$ and (b) $w = 750nm$.

center wavelength $1550nm$, independent of the waveguide. The reason for this behavior is not clear, and it did not appear in the same measurements when no attenuator was used.

Furthermore, from the estimated peak powers of the attenuated pulses shown on Figure 5.13, the idea was to then place a tunable attenuator that would allow us to choose any other value for the peak power between $0W$ and the values on the Figure. We did so with the intent of studying the same limiting phenomenon that was observed for picosecond pulses and that is clearly predicted for the parameters here. We failed however to observe any significant spectral distortion when a second attenuator was placed after the first one, and no significant limiting was observed either.

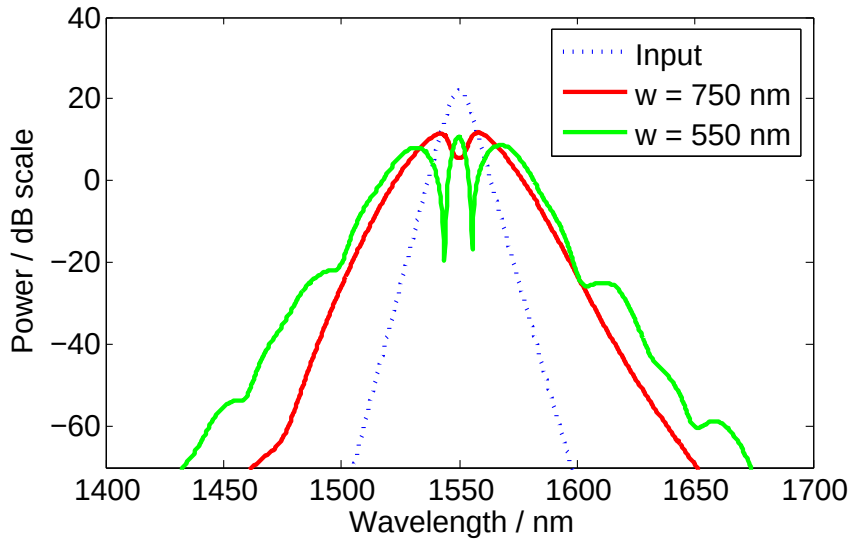

Figure 5.14: Modeling results for the $350fs$, $2.53W$ pulses propagating in the Si wires.

5.3 Summary

In this chapter, we have reported the experimental results obtained in this work. The results with picosecond pulses tend to correlate very well with the theory we developed in previous chapters. Our results with much shorter pulses have proven rather difficult to interpret as resulting from any of the effects we described earlier. This, we believe, results from the fact that our laser source cannot be characterized properly. Still, the obtained results confirm the strong nonlinear interaction between the pulses and our Si wires.

Chapter 6

Conclusion and Outlook

Though silicon cannot efficiently emit light, it can guide it an interact with it through its strong nonlinearities. We set out to investigate these nonlinear interactions in Si wire waveguides, with the aim of determining conditions under which they would lead to efficient continuum generation.

We have in the current work, journeyed through how silicon can be used for engineering the spectrum of incident short pulses through nonlinear optical interactions. We have presented a thorough description of the physical phenomena that affect nonlinear light propagation in Si photonic wires. We have implemented a model (from a similar one used for fibres) in an attempt to understand and predict the result of ultrashort pulse propagation in Si wires experiments.

Most importantly however, we have carried out a great number of experiments with the intent to not only further understand the physics of nonlinear light propagation in wire waveguides, but also to be able to engineer the features of the output spectra in such experiments. Part of the results we obtained agree quite well with what can be deduced from our modeling results, and part of them do not. We do believe the inputs have not been optimized to reach the objectives we were set out for. In a time frame as short as a few months, acquiring a femtosecond source , correctly characterizing it and going through all the troubleshooting with the aim to optimize it for our experiments have proven to be a difficult task, albeit not an impossible one.

Further work on this exciting topic in our group would first focus on a full and thorough characterization of the experimental equipment available in the lab. With the foundations laid in the present work, experimental demonstration of continuum generation in Si wires would simply require that the pumping source be chosen properly, and that the coupling of light to the waveguide be cleared of unknowns such as

possible chirp from the gratings, though such unknowns could eventually prove to be useful. Further work can be also carried out first by implementing a full description of the coupled-mode theory involving simultaneous propagation of pulses at different wavelengths, and then find conditions under which they would lead to broadband light generation or other useful effects.

Appendix A

Dispersion coefficients for the wire waveguides used in this work

Here are the dispersion coefficients at $1550nm$ for the waveguides studied in this work. Dispersion plots obtained from Fimmwave simulations can be seen on Figures 2.5 and 2.6.

Waveguide width	$\beta_2(ps^2/m)$	$\beta_3(ps^3/m)$	ZDW(nm)
350 nm	1.439	-0.2506	1542
400 nm	-5.037	-8.198×10^{-3}	1661.5
450 nm	-3.999	9.942×10^{-3}	1781
500 nm	-2.957	1.071×10^{-2}	1886
550 nm	-2.068	9.025×10^{-3}	1191 and 1997
600 nm	-1.392	7.358×10^{-3}	1259
650 nm	-0.869	5.775×10^{-3}	1330
700 nm	-0.469	4.594×10^{-3}	1408
750 nm	-0.157	3.653×10^{-3}	1495
800 nm	9.234×10^{-2}	2.886×10^{-3}	1591
850 nm	0.294	2.279×10^{-3}	1702

Bibliography

[1] X. Chen, N. C. Panoiu, and R. M. Osgood Jr., "Theory of Raman-mediated pulsed amplification in silicon-wire waveguides," IEEE J. Quantum Electron. **42,** 160–170 (2006).

[2] J. I. Dadap, N. C. Panoiu, Xiaogang Chen, I-Wei Hsieh, Xiaoping Liu, Cheng-Yun Chou, E. Dulkeith, S. J. McNab,Fengnian Xia, W. M. J. Green, L. Sekaric, Y. A. Vlasov, and R. M. Osgood, Jr., " Nonlinear-optical phase modification in dispersion-engineered Si photonic wires" Optics Express **16**, 2, 1280–1299 (2008)

[3] Alan D. Bristow, Nir Rotenberg and Henry M. van Driel , " Two-photon absorption and Kerr coefficients of silicon for 850 - 2200 nm" Appl. Phys. Lett. **90**, 191104 (2007)

[4] Pieter Dumon, " Ultra-compact Integrated Optical Filters in Silicon-On-Insulator by Means of Wafer-Scale Technology," PhD. Thesis, UGent INTEC,(2007)

[5] M. Dinu, F. Quochi and H. Garcia "Third-order nonlinearities in silicon at telecom wavelengths " Appl. Phys. Lett. **82**, p2954 (2007)

[6] Haisheng Rong, Richard Jones, Ansheng Liu, Oded Cohen, Dani Hak, Alexander Fang and Mario Paniccia, "A Contnuous-wave Raman Silicon Laser", Nature **433**, 725 – 728 (2005)

[7] R. M. Osgood, Jr., N. C. Panoiu, J. I. Dadap, Xiaoping Liu, Xiaogang Chen, I-Wei Hsieh, E. Dulkeith, W. M. J. Green and Y. A. Vlasov, "Engineering nonlinearities in nanoscale optical systems: physics and applications in dispersion-engineered silicon nanophotonic wires", Advances in Optics and Photonics **1**, 162 – 235 (2009)

[8] Q. Lin, Oskar J. Painter and Govind P. Agrawal "Nonlinear optical phenomena in silicon waveguides: Modeling and applications", Optics Express **15**, 25, 16604–16644 (2007)

[9] R. A. Soref and B. R. Bennett "Electrooptical effects in silicon ", IEEE J. Quantum Electron.**23** 123–129 (1987)

[10] Gino Priem, "Nonlinear Behaviour in Nanophotonic Waveguides and Resonators for Ultrafast Signal Processing", PhD Thesis, UGent INTEC, (2006)

[11] Roel Baets and Irina Veretenicoff, Nonlinear and Quantum Optics course, UGent INTEC

[12] B. A. Daniel and G. P. Agrawal, " Dependence of dispersive and birefringence properties of silicon nanowires on waveguide dimensions", Opt. Lett.**35**, 190–192 (2010)

[13] C. Koos, L. Jacome, C. Poulton, J. Leuthold and W. Freude, "Nonlinear silicon-on-insulator waveguides for all-optical signal processing", Optics Express **15**, No. 10, 5976–5990 (2007).

[14] Paul N. Butcher and David Cotter, " The elements of nonlinear Optics", Cambridge University press, 1990

[15] A. Liu, H. Rong, M. Paniccia, O. Cohen, and D. Hak, "Net optical gain in a low loss silicon-on-insulator waveguide by stimulated Raman scattering," Opt. Express **12**, 4261–4268 (2004).

[16] T. K. Liang and H. K. Tsang,"Efficient Raman amplificationin silicon-on-insulator waveguides" Appl. Phys. Lett. **85**, 3343–3345 (2004)

[17] B. M. Caradoc-Davies, "Vortex dynamics in Bose-Einstein condensates," Ph. D. dissertation, Univ. Otago, Dunedin, New Zealand, 2000. [Online]. Available: http://www.physics.otago.ac.nz/bec2/bmcd/phdthesis/

[18] Johan Hult, "A Fourth-Order Runge-Kutta in the Interaction Picture Method for Simulating Supercontinuum Generation in Optical Fibers ," IEEE J. Lightwave Technol. **25**, 12 (DEC), 3770-3775 (2007)

[19] J. M. Dudley, G. Genty, and S. Coen, "Supercontinuum generation in photonic crystal fiber," Rev. Mod. Phys. **78**, no. 4, pp. 1135 - 1184,(2006)

[20] J. M. Dudley and J. R. Taylor, "Supercontinuum Generation in Optical Fibers," Chapter 3 by J. C. Travers, M. H. Frosz and J. M. Dudley, p32, Cambride University Press (2010)

[21] Agrawal G. P. " Nonlinear Fiber Optics" , 4th edn. San Diego: Academic Press (2007).

[22] Lianghong Yin, Qiang Lin, and Govind P. Agrawal, " Soliton fission and supercontinuum generation in silicon waveguides", Optics Letters **32**, No. 4, 391–393 (2007)

[23] Lianghong Yin and Govind P. Agrawal, " Impact of two-photon absorption on self-phase modulation in silicon waveguides, "Optics Letters **32**, No 14, 2031–2033 (2007).

[24] Eric Dulkeith, Yurii A. Vlasov, Xiaogang Chen, Nicolae C. Panoiu, and Richard M. Osgood, Jr."Self-phase modulation in submicron silicon-on-insulator photonic wires,"Opt. Express **14**, 5524–5534 (2006)

[25] I-Wei Hsieh, Xiaogang Chen, Jerry I. Dadap, Nicolae C. Panoiu, and Richard M. Osgood, Jr., Sharee J. McNab and Yurii A. Vlasov "Ultrafast pulse self-phase modulation and third-order dispersion in Si photonic wire-waveguides, " Optics Express **14**, No 25, 12380–12387 (2006)

[26] J. Zhang, Q. Lin, G. Piredda, R. W. Boyd, G. P. Agrawal, and P. M. Fauchet, "Optical solitons in a silicon waveguide," Optics Express **15**, 7682–7688 (2007).

[27] Ö. Boyraz, P. Koonath, V. Raghunathan, and B. Jalali, "All optical switching and continuum generation in silicon waveguides," Optics Express **12**, 4094–4102 (2004).

[28] Neil Akhmediev and Magnus Karslson, "Cherenkov radiation emitted by solitons in optical fibers, " Phys. Rev. A. **51** 2602 (1995).

[29] I-Wei Hsieh,Xiaogang Chen, Xiaoping Liu, Jerry I. Dadap, Nicolae C. Panoiu, Cheng-Yun Chou, Fengnian Xia, William M. Green,Yurii A. Vlasov, and Richard M. Osgood, Jr."Supercontinuum generation in silicon photonic wires,"Optics Express **15**, No 23, 15242–15249 (2007).

[30] Nicolae C. Panoiu, Xiaogang Chen, and Richard M. Osgood, Jr., " Modulation instability in silicon photonic nanowires", Optics Letters **31**, No 24, 3609–3611

[31] Richard L. Espinola, Jerry I. Dadap, Richard M. Osgood, Jr., Sharee J. McNab and Yurii A. Vlasov " C-band wavelength conversion in silicon photonic wire waveguides", Optics Express **13** No 11, 4341–4349 (2005)

[32] H K Tsang and Y Liu, " Nonlinear optical properties of silicon waveguides," Semicond. Sci. Technol. **23**, 064007 (2008) doi:10.1088/0268-1242/23/6/064007